AGU PUBLICATIONS

Tectonics

RESEARCH ARTICLE

10.1002/2017TC004681

Geometry of a large-scale, low-angle, midcrustal thrust (Woodroffe Thrust, central Australia)

S. Wex[1], N. S. Mancktelow[1], F. Hawemann[1], A. Camacho[2], and G. Pennacchioni[3]

[1]Department of Earth Sciences, ETH Zurich, Zurich, Switzerland, [2]Department of Geological Sciences, University of Manitoba, Winnipeg, Manitoba, Canada, [3]Department of Geosciences, University of Padova, Padova, Italy

Key Points:

- The Woodroffe Thrust preserves a midcrustal to lower crustal shearing history in the central Musgrave Block
- The syndeformational geometry of the thick-skinned Woodroffe Thrust was shallowly dipping (≤6°) over ≥60 km in the direction of thrusting
- Intracontinental shortening in Australia at circa 560–520 Ma was in part accommodated by in-sequence underthrusting

Supporting Information:

- Supporting Information S1

Correspondence to:
N. Mancktelow,
neil.mancktelow@erdw.ethz.ch

Citation:
Wex, S., N. S. Mancktelow, F. Hawemann, A. Camacho, and G. Pennacchioni (2017), Geometry of a large-scale, low-angle, midcrustal thrust (Woodroffe Thrust, central Australia), *Tectonics*, *36*, 2447–2476, doi:10.1002/2017TC004681.

Received 30 MAY 2017
Accepted 19 AUG 2017
Accepted article online 25 AUG 2017
Published online 13 NOV 2017

Abstract The Musgrave Block in central Australia exposes numerous large-scale mylonitic shear zones developed during the intracontinental Petermann Orogeny around 560–520 Ma. The most prominent structure is the crustal-scale, over 600 km long, E-W trending Woodroffe Thrust, which is broadly undulate but generally dips shallowly to moderately to the south and shows an approximately top-to-north sense of movement. The estimated metamorphic conditions of mylonitization indicate a regional variation from predominantly midcrustal (circa 520–620°C and 0.8–1.1 GPa) to lower crustal (~650°C and 1.0–1.3 GPa) levels in the direction of thrusting, which is also reflected in the distribution of preserved deformation microstructures. This variation in metamorphic conditions is consistent with a south dipping thrust plane but is only small, implying that a ≥60 km long N-S segment of the Woodroffe Thrust was originally shallowly dipping at an average estimated angle of ≤6°. The reconstructed geometry suggests that basement-cored, thick-skinned, midcrustal thrusts can be very shallowly dipping on a scale of many tens of kilometers in the direction of movement. Such a geometry would require the rocks along the thrust to be weak, but field observations (e.g., large volumes of syntectonic pseudotachylyte) argue for a strong behavior, at least transiently. Localization on a low-angle, near-planar structure that crosscuts lithological layers requires a weak precursor, such as a seismic rupture in the middle to lower crust. If this was a single event, the intracontinental earthquake must have been large, with the rupture extending laterally over hundreds of kilometers.

1. Introduction

Large-scale deformation in contractional regimes is associated with either thick- or thin-skinned tectonics [*Coward*, 1983]. Thin-skinned tectonics is typically characterized by an alternating flat-ramp thrust geometry, while thick-skinned tectonics is marked by basement-cored nappes. For both models, simple application of the Coulomb criterion for shear failure [e.g., *Anderson*, 1905, 1951] predicts that the thrust plane should initiate at an angle of ~30° to the axis of maximum shortening [*Healy et al*., 2012]. The reactivation of already existing fault planes should also be favored at these Andersonian attitudes of ~30° [*Sibson*, 1990, 2012]. In the case of fault initiation, this value reflects the angle of internal friction, whereas, in the case of fault reactivation, it reflects the angle of external (sliding) friction [*Handin*, 1969]. These parameters are, strictly speaking, not the same but similar for most rock types at medium- to high-grade conditions [*Byerlee*, 1978; *Jäger and Cook*, 1979]. As a direct consequence, thrusts are generally predicted to dip at ~30° to the horizontal [e.g., *Ramsay and Huber*, 1987; *Twiss and Moores*, 2007; *Fossen*, 2016]. This assumption has been confirmed by analogue sandbox experiments [e.g., *Davis et al*., 1983; *Malavieille*, 1984], by rock deformation experiments [e.g., *Donath*, 1961], and by geophysical data [e.g., *Smithson et al*., 1978; *Brewer et al*., 1980; *Brewer and Smythe*, 1984]. Sandbox models are an oversimplification of natural deformation processes, whereas geophysical methods can only predict the present-day geometry of a fault at depth but not the initial fault geometry and its evolution during thrusting. These issues can only be resolved by directly studying natural examples and trying to understand their spatial and temporal evolution. The Musgrave Block in central Australia (Figure 1), provides an ideal framework for testing the geometrical assumptions summarized above. This area experienced a major intracontinental compressional event at circa 560–520 Ma (Petermann Orogeny) involving an early phase of thin-skinned deformation [*Scrimgeour et al*., 1999] and subsequent thick-skinned tectonics [*Lambeck and Burgess*, 1992; *Camacho and McDougall*, 2000]. One of the largest of the thick-skinned shear zones is the crustal-scale Woodroffe Thrust [*Major*, 1970], which is well exposed in the central Musgrave Block over 150 km along strike and ~60 km in the direction of thrusting (Figure 2), making it an ideal candidate for studying thrust geometry. The geometry, evolution, and kinematics of the Woodroffe Thrust are the focus of this paper.

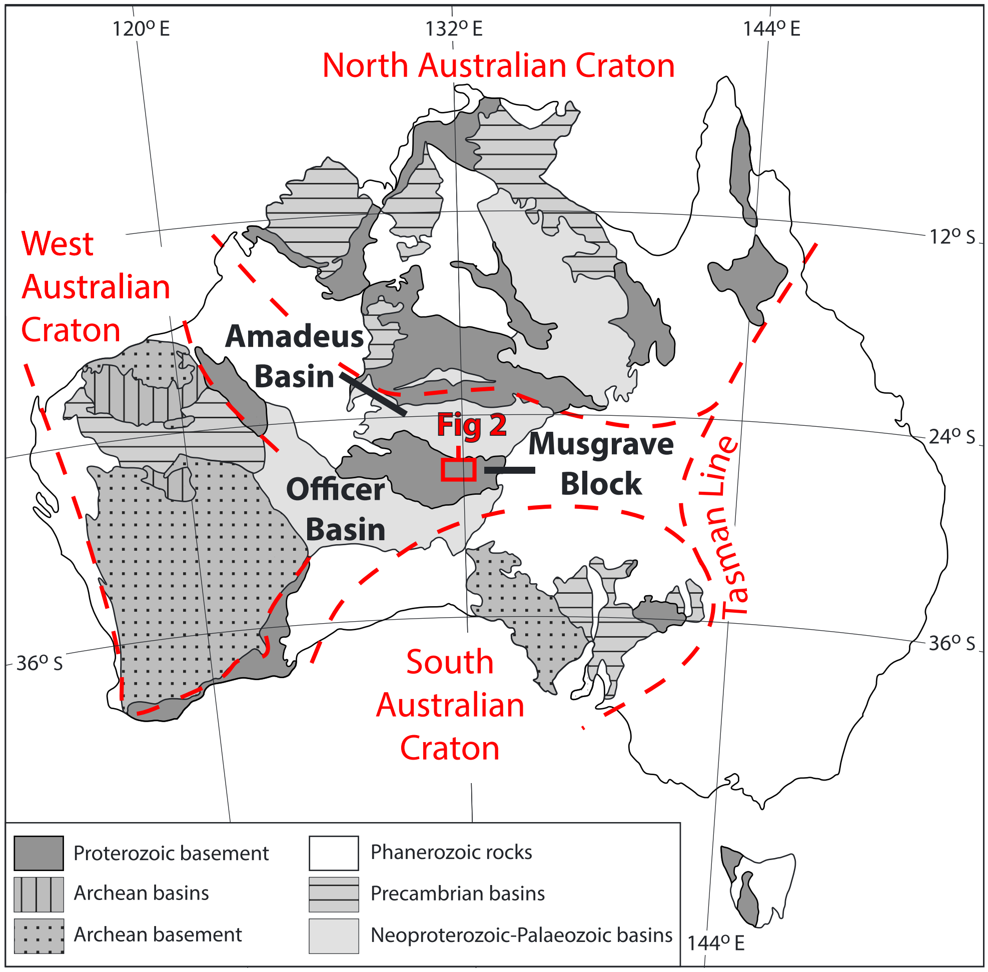

Figure 1. Distribution of Archean and Proterozoic basement blocks in relation to Neoproterozoic to early Phanerozoic sedimentary basins in Australia (modified after *Wyborn et al.* [1987], *Camacho and McDougall* [2000], and *Evins et al.* [2010]).

2. Geology

Most of the Australian continent consists of the Paleoproterozoic north, west, and south Australian cratons (Figure 1). Each of these units was assembled from various crustal fragments of Archean crust by ~1830 Ma, with all three cratons in turn amalgamated at ~1300 Ma as an early component of the supercontinent Rodinia [*Myers et al.*, 1996]. The Musgrave Block is bounded to the north by the Neoproterozoic to Palaeozoic Amadeus Basin and to the south and west by the Neoproterozoic to Palaeozoic Officer Basin [*Major and Conor*, 1993]. Numerous large-scale mylonitic shear zones are preserved throughout the Musgrave Block [*Major*, 1970; *Collerson et al.*, 1972; *Bell*, 1978; *Major and Conor*, 1993; *Camacho et al.*, 1997; *Scrimgeour et al.*, 1999; *Edgoose et al.*, 2004]. The most prominent structure is the over 600 km long, E-W striking Woodroffe Thrust [*Major*, 1970], which developed during the Petermann Orogeny around 560–520 Ma [*Maboko et al.*, 1992; *Camacho and Fanning*, 1995]. On a global scale, this deformation phase broadly corresponds to the Pan-African event [*Camacho et al.*, 1997]. However, the processes that led to the transfer of stresses from the Australian plate margins to the interior, as well as the weakening processes that led to strain localization in such an intracontinental setting, remain controversial [*Sandiford and Hand*, 1998; *Hand and Sandiford*, 1999; *Braun and Shaw*, 2001; *Roberts and Houseman*, 2001; *Camacho et al.*, 2002; *Raimondo et al.*, 2014]. The Woodroffe Thrust separates the footwall Mulga Park Subdomain from the hanging wall Fregon Subdomain [*Edgoose et al.*, 1993; *Major and Conor*, 1993] (Figure 2). Both subdomains are dominantly comprised of quartzo-feldspathic gneisses and granitoids, with subordinate metadolerites, mafic gneisses, and metapelites. Rare quartzites, amphibolites, and schists are restricted to the Mulga Park

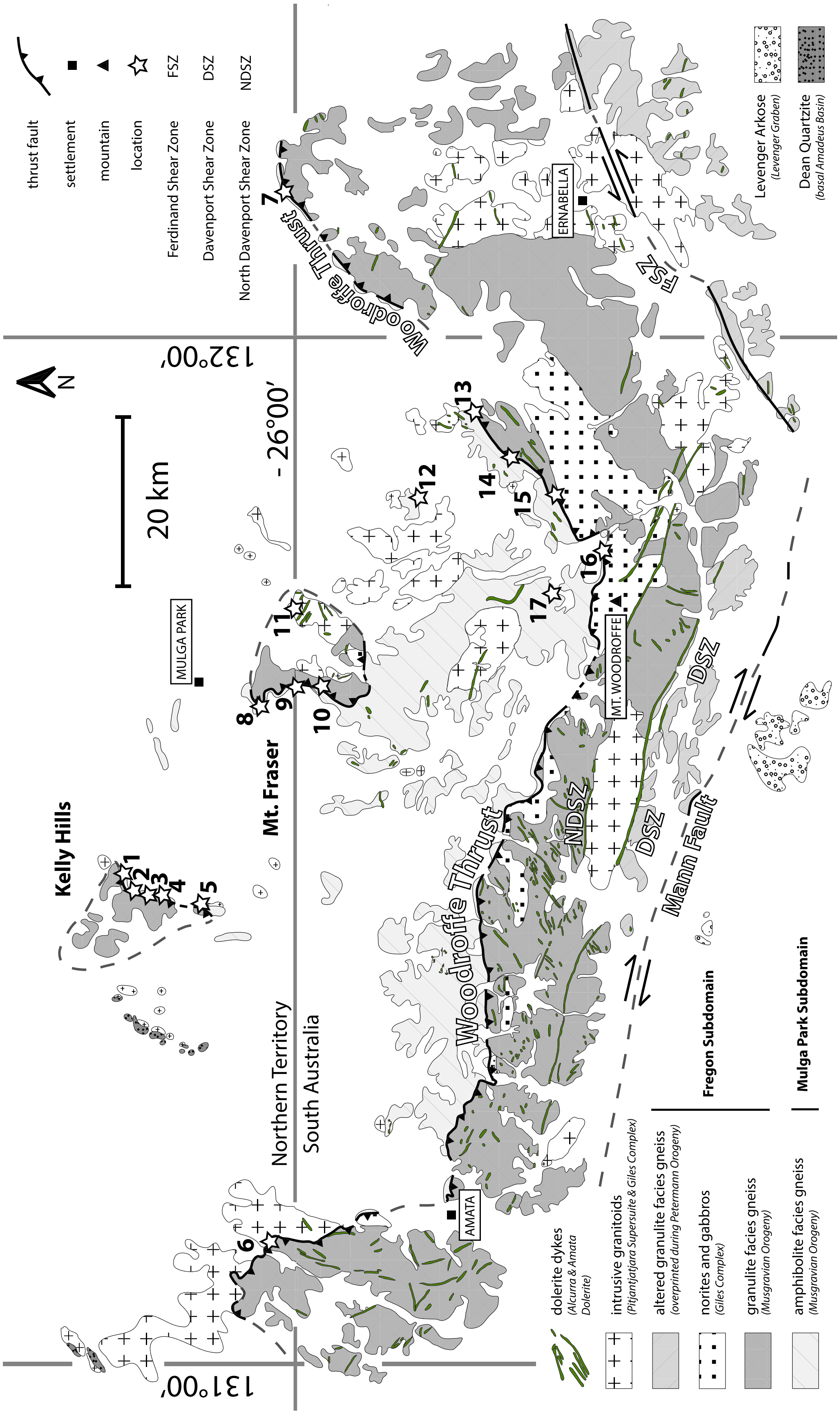

Figure 2. Geological map of the central Musgrave Block (modified after *Sprigg et al.* [1959], *Major et al.* [1967], and *Young et al.* [2002]).

Subdomain [*Collerson et al*., 1972; *Major*, 1973; *Major and Conor*, 1993; *Scrimgeour and Close*, 1999]. Similar structural and magmatic histories prior to their juxtaposition suggest that the two units represent different crustal levels of the same terrane, rather than being distinctly different blocks [*Camacho and Fanning*, 1995; *Scrimgeour et al*., 1999].

The protoliths of the gneisses were dominantly felsic volcanics, sediments, and intrusives with depositional or emplacement ages of ~1550 Ma [*Gray*, 1977, 1978; *Gray and Compston*, 1978; *Maboko et al*., 1991; *Sun and Sheraton*, 1992; *Major and Conor*, 1993; *Camacho and Fanning*, 1995]. Widespread felsic magmatism (Pitjantjatjara Supersuite; circa 1190 to 1120 Ma) was syntectonic to posttectonic to the ~1200 Ma Musgravian Orogeny, with regional metamorphism of upper amphibolite and granulite facies in the Mulga Park and Fregon Subdomains, respectively [*Gray*, 1978; *Moore and Goode*, 1978; *Maboko et al*., 1991; *Sun and Sheraton*, 1992; *Major and Conor*, 1993; *Camacho and Fanning*, 1995; *Camacho et al*., 1997; *Scrimgeour et al*., 1999; *Edgoose et al*., 2004; *Smithies et al*., 2011]. Subsequent episodes of bimodal magmatism (Giles Complex, including the Alcurra Dolerite swarm) and mafic magmatism (Amata Dolerite swarm) occurred at circa 1080 to 1050 Ma and ~800 Ma, respectively [*Camacho et al*., 1991, 1997; *Edgoose et al*., 1993; *Zhao and McCulloch*, 1993; *Zhao et al*., 1994; *Ballhaus and Glikson*, 1995; *Clarke et al*., 1995; *Sun et al*., 1996]. The second major deformation phase affecting the Musgrave Block was the Petermann Orogeny (circa 560–520 Ma), during which the crustal-scale Woodroffe Thrust developed, together with other large-scale ductile shear zones, such as the Mann, Ferdinand, and Hinckley Faults, the Davenport Shear Zone, and the Wankari and Piltardi Detachment Zones [*Major*, 1970; *Collerson et al*., 1972; *Pharaoh*, 1990; *Major and Conor*, 1993; *Camacho et al*., 1995, 1997; *Scrimgeour et al*., 1999] (Figure 2). In the hanging wall of the Woodroffe Thrust, the metamorphic conditions attributed to the Petermann Orogeny are of high-pressure amphibolite to subeclogite facies, ranging from 700–750°C and 1.2–1.4 GPa in the western part [*Clarke et al*., 1995; *White and Clarke*, 1997; *Scrimgeour and Close*, 1999] to 650–700°C and ~1.2 GPa in the east [*Maboko et al*., 1989, 1991; *Ellis and Maboko*, 1992; *Camacho et al*., 1997]. In the eastern part, which covers our study area (Figure 2), *Maboko et al*. [1989, 1991] and *Ellis and Maboko* [1992] originally attributed these pressures and temperatures to isobaric cooling during the Musgravian Orogeny. However, this overprint was reinterpreted by *Camacho et al*. [1997] and *Camacho and McDougall* [2000] to be the result of rapid burial and exhumation during the Petermann Orogeny. Conditions below and along the Woodroffe Thrust have generally been estimated at upper greenschist to lower amphibolite facies [*Maboko et al*., 1992; *Camacho and Fanning*, 1995] but have previously not been precisely determined. Evidence for the influence of the mid-Palaeozoic Alice Springs Orogeny is sparse [*Edgoose et al*., 2004] and, in the study area, seems to be limited to the development of discretely localized thin chlorite-epidote-actinolite veins and narrow zones of distinct bleaching along fractures crosscutting the high-grade fabric.

3. Methodology

The hanging wall, footwall, and numerous transects across the mylonitic zone of the Woodroffe Thrust were studied and sampled in detail for analysis (Figure 2). The surface intersection with the topography and field measurements of the foliation within the thrust zone were processed in GeoModeller (Intrepid Geophysics) to generate a first-order model visualizing the three-dimensional present-day geometry of the thrust surface. For microstructural and textural analysis with the standard polarizing microscope and with the scanning electron microscope, thin sections were prepared from sample slabs cut perpendicular to the foliation and parallel to the stretching lineation. Mineral compositions were measured and mapped with a JEOL JXA-8200 electron probe microanalyzer and used to constrain the metamorphic conditions via conventional geothermobarometry. Polymorphic minerals were distinguished using Raman spectroscopy and electron backscatter diffraction (EBSD). Mineral abbreviations are after *Whitney and Evans* [2010]. Sample/outcrop coordinates are given in the world geodetic system 1984. Orientation measurements of structural elements are corrected for magnetic declination. A detailed description of all methods utilized is outlined in the supporting information A.

4. Field Observations

4.1. Woodroffe Thrust

The mylonitic zone of the Woodroffe Thrust is defined by an association of protomylonites, mylonites, ultramylonites, and blastomylonites (Figures 3a–3e), with the degree of mylonitization decreasing into the

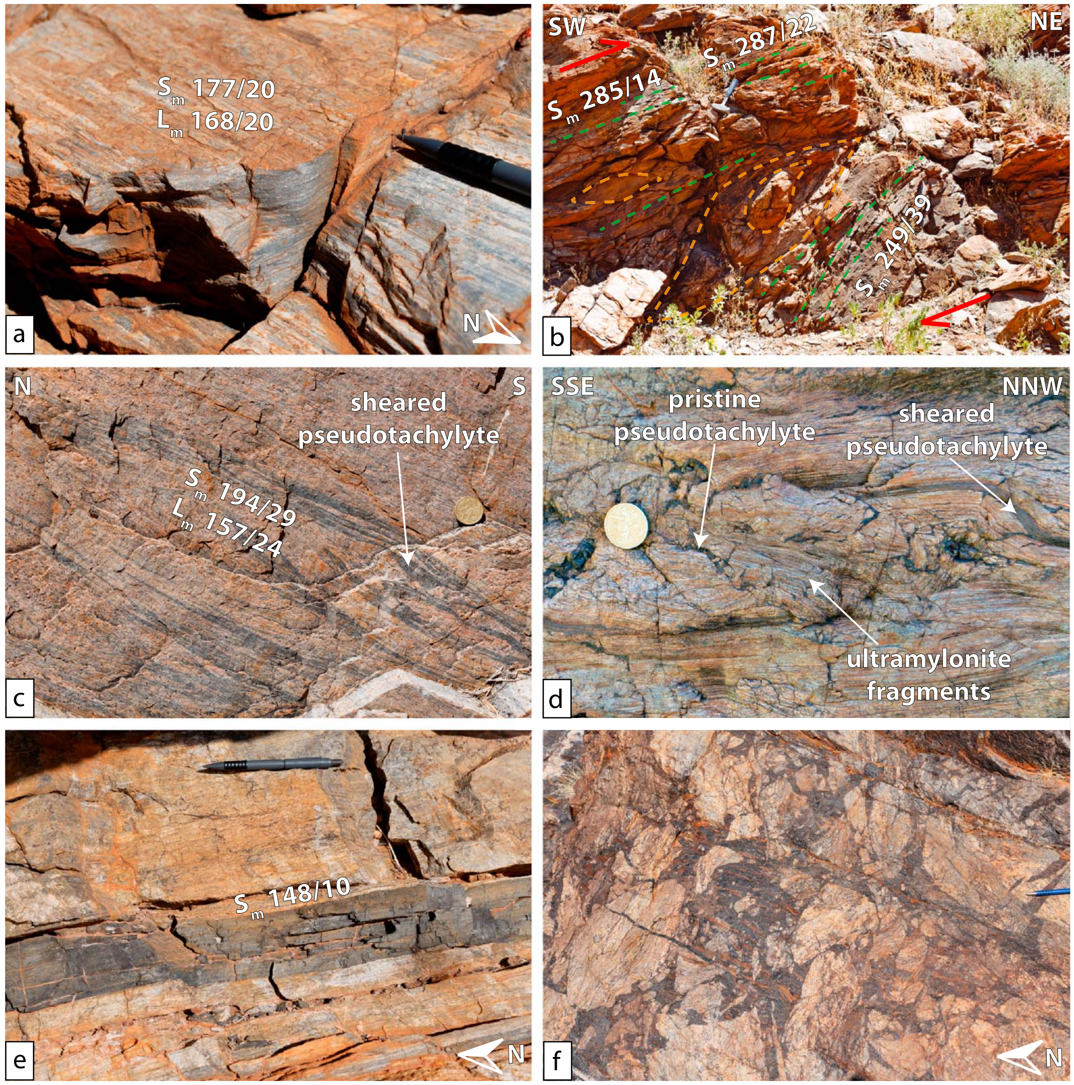

Figure 3. Field photographs of the Woodroffe Thrust, including the orientations of the mylonitic foliation (S_m) and stretching lineation (L_m), given as dip direction and dip angle and plunge direction and plunge angle, respectively. (a) Ultramylonites. Outcrop NW13-246 (coordinates: 131.77436, −26.30773; location 16 in Figure 2). (b) Asymmetrically deformed low-strain domains (orange dashed line) and the changing dip in foliation (green dashed line) indicate a top-to-NNE movement during shearing. Outcrop NW13-260 (coordinates: 131.45391, −25.84531; location 2 in Figure 2). (c) Foliation-parallel sheared pseudotachylyte. Outcrop NW13-242 (coordinates: 131.77316, −26.30622; location 16 in Figure 2). (d) Pristine pseudotachylyte breccia developed in an ultramylonitic host rock. Outcrop SW13-162 (coordinates: 131.77444, −26.30781; location 16 in Figure 2). (e) Foliated dolerite dyke within felsic mylonites. Outcrop NW13-186 (coordinates: 131.87837, −26.20970; location 14 in Figure 2). (f) Pristine pseudotachylyte breccia in the hanging wall granulites of the Woodroffe Thrust. Outcrop NW13-470 (coordinates: 132.14340, −25.99225; location 7 in Figure 2).

footwall. The thickness of this zone increases from several tens to a few hundred meters in the north (locations 1–10 in Figure 2) to several hundreds of meters in the south (locations 13–16 in Figure 2). Low-strain domains are common (Figure 3b) and present at all scales. Pseudotachylytes and dolerite dykes are generally overprinted by the mylonitic foliation (Figures 3c–3e), with pristine pseudotachylytes that crosscut and brecciate the mylonitic fabric only rarely preserved (Figure 3d). However, the first few hundred meters of the immediate hanging wall of the Woodroffe Thrust include large amounts of pseudotachylytes (Figure 3f), which are mostly unsheared but marginally reworked into the adjacent footwall mylonites. The sheared pseudotachylytes were in turn crosscut by undeformed pseudotachylyte.

The mylonitic foliation is shallowly dipping and defines, on the scale of the investigated field area, a broad half-dome structure, which roughly dips toward the south (Figures 4 and 5). In the northern and central

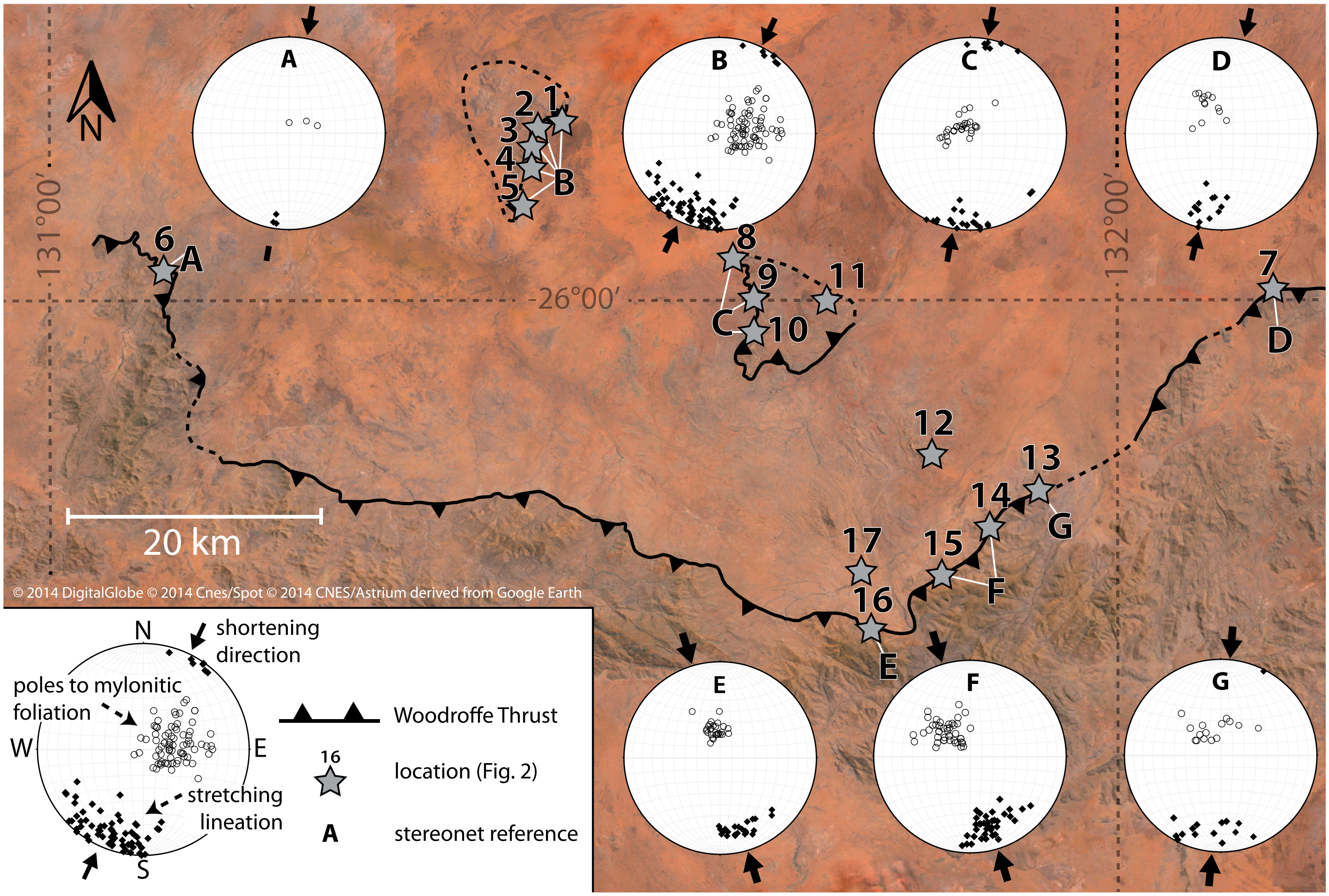

Figure 4. Satellite imagery of the central Musgrave Block. Orientation data of the mylonitic foliation and stretching lineation are projected in lower hemisphere Schmidt nets (A-G). The measurements indicate N-S shortening, locally varying between NNE-SSW and NNW-SSE.

part of the study area, the thrust plane is generally flat but undulate and characterized by two local depressions, which create the Kelly Hills and Mount Fraser klippen (Figure 5). In the south, the thrust plane steepens toward an average dip of ~30° (locations 13–16 in Figure 5).

Stretching lineations indicate a general N-S displacement, with a local span between NNE-SSW and NNW-SSE (Figure 4). Folds with a steep fold axial plane (associated with sheared pseudotachylytes) suggest a component of WNW-ESE shortening postdating the development of the Woodroffe Thrust mylonites (Figure 6). In location 11 (Figure 2), numerous isolated, approximately strike-slip shear zones can be referred to two main groups, whose change in kinematics also reflect two different shortening directions, respectively, NNE-SSW and WNW-ESE (Figure 7). No crosscutting relationships were observed between the two sets of shear zones.

Movement sense is generally top-to-north in the main mylonitic zone (Figures 3b, 9b, and 10a), whereas, farther into the less strained hanging wall and footwall, isolated shear zones occasionally show a top-to-south shear sense. Within heterogeneously deformed mylonites associated with the Woodroffe Thrust in the Amata region (western edge of Figure 2), *Bell and Johnson* [1992] also observed local reverses in the shear sense occurring on scales ranging from outcrop to individual thin sections.

4.2. Top-to-West Mylonites

A distinctly different mylonitic zone, several hundreds of meters wide, has been recognized in the southern locations 13–15 (Figure 2). These mylonites can be distinguished from those of the Woodroffe

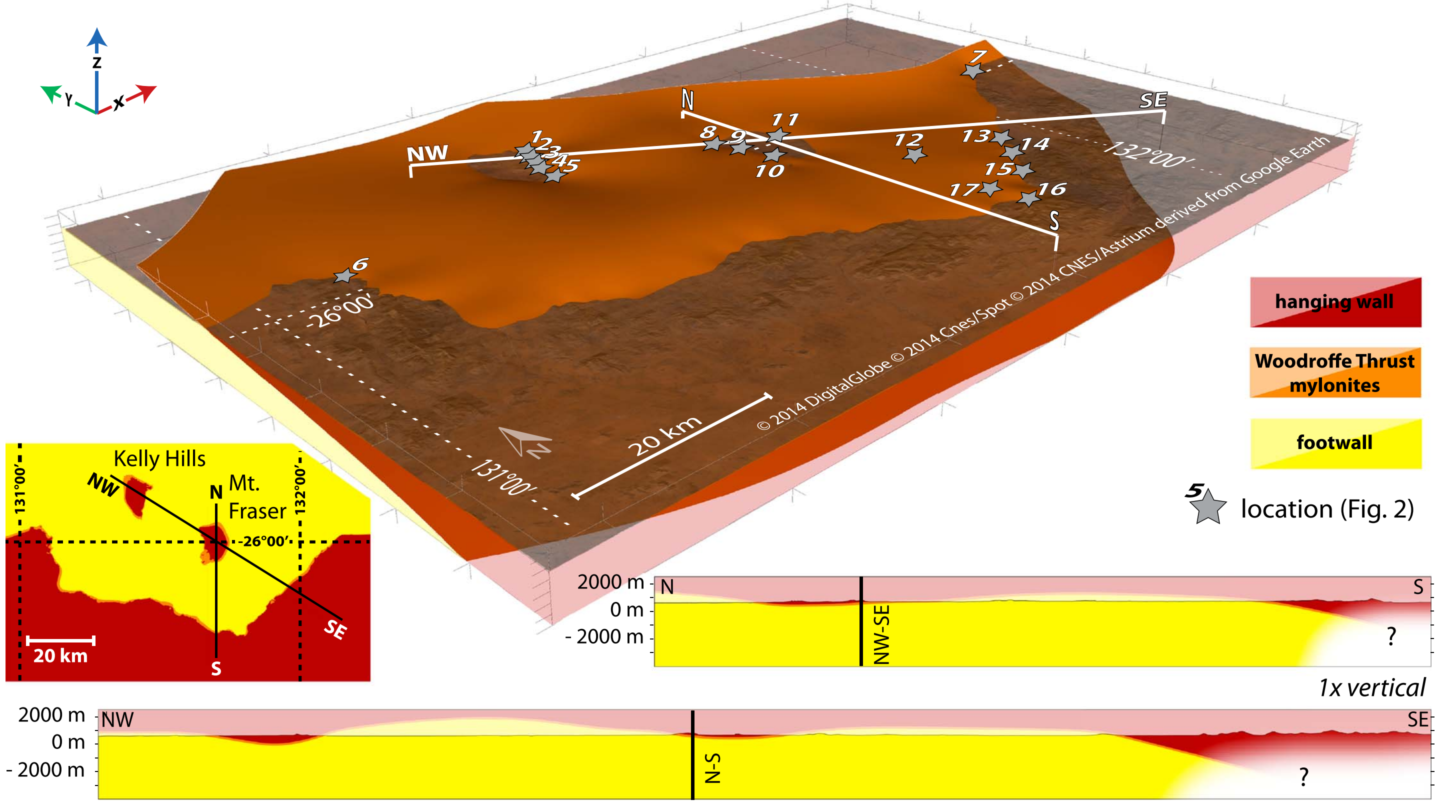

Figure 5. Three-dimensional model of the present-day half-dome-shaped geometry of the Woodroffe Thrust. In the model, three units are distinguished: hanging wall, mylonites, and footwall. Normal faulting is not considered. The straight and planar geometry of the Woodroffe Thrust at the western margin of the model is not correct but arises due to the lack of input constraints.

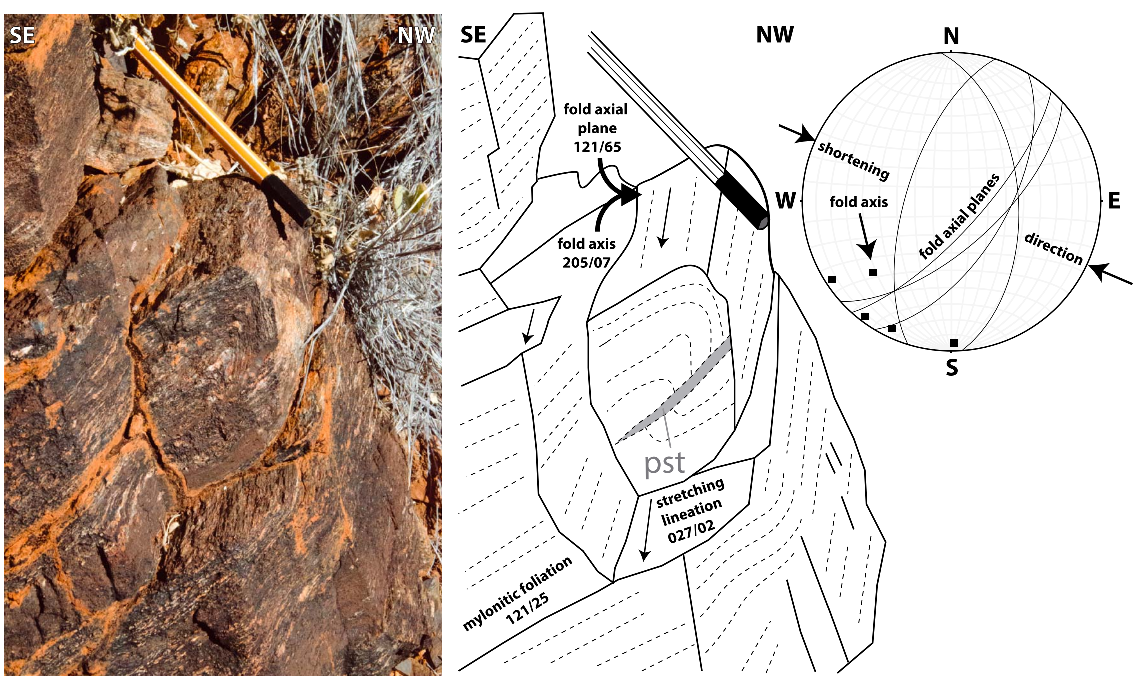

Figure 6. (left) Field photograph and (right) sketch of Woodroffe Thrust mylonites folded with a steep axial fold plane. Pristine pseudotachylyte (pst) is emplaced parallel to the fold axial plane. Thin arrows indicate the stretching lineation. A compilation of several outcrops is presented in a lower hemisphere Schmidt net, indicating WNW-ESE shortening. Outcrop SW14-179 (coordinates: 131.92603, −26.17661; location 13 in Figure 2).

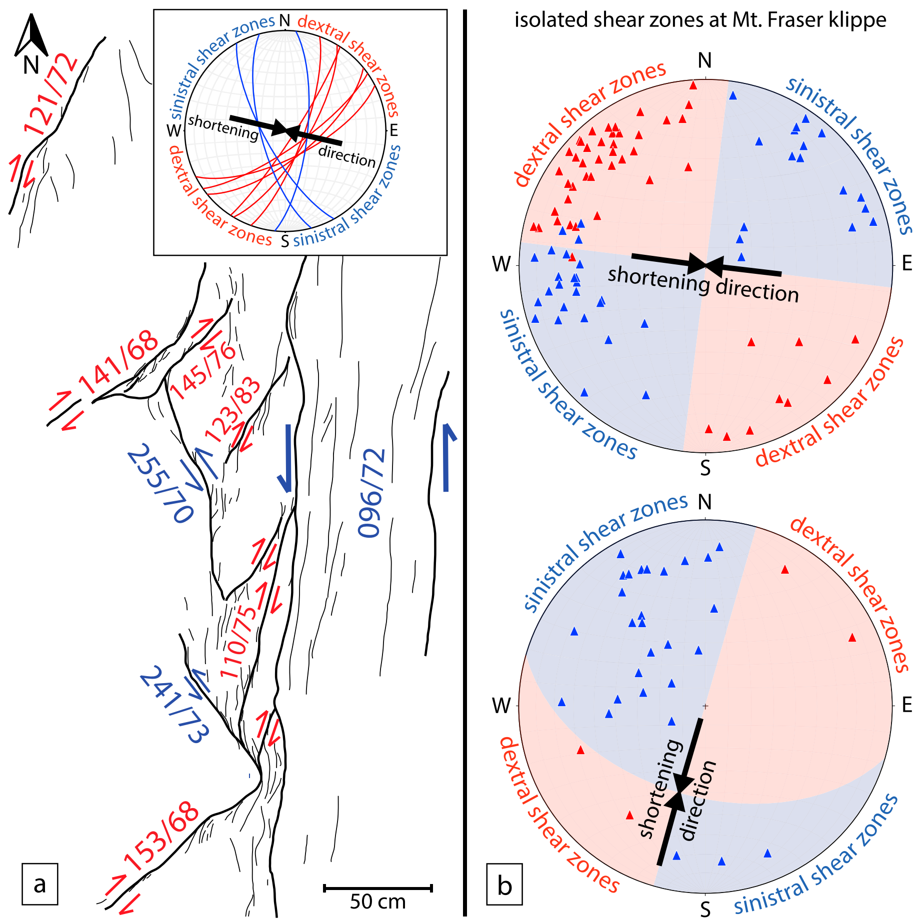

Figure 7. Isolated shear zones in the hanging wall of the Woodroffe Thrust from the Mount Fraser klippe (location 11 in Figure 2). Orientation data are plotted in lower hemisphere Schmidt nets. (a) Outcrop sketch of sinistral and dextral shear zones in a little deformed granite. The changing sense of shear is consistent with WNW-ESE shortening. Outcrop SW13-202 (coordinates: 131.74255, −26.00140; location 11 in Figure 2). (b) Poles of sinistral and dextral shear zones are separated into two groups, one associated with a WNW-ESE (top) and another with a NNE-SSW (bottom) oriented shortening direction. No crosscutting relationships were observed between the two sets of shear zones.

Thrust by (1) their coarser grain size, (2) the roughly ESE dipping foliation and ENE to ESE plunging stretching lineation (Figure 8a), (3) the absence of the typical, prominent stretching lineation on the foliation plane (Figure 8b), (4) their top-to-west shear sense (Figure 8c), and (5) the lack of pseudotachylyte. These mylonites overprint the dolerite dykes which, in the footwall, are folded with roughly NE-SW trending fold axial planes (Figure 8a). Top-to-west mylonites and folded dolerites are themselves overprinted by, and oriented into parallelism with, the Woodroffe Thrust. To our knowledge, this deformation phase, which implies significantly different kinematics to that of the Woodroffe Thrust, has not been previously described in the study area. This phase possibly correlates with the greenschist to amphibolite facies D5 deformation event of *Clarke* [1992] farther west in the Tomkinson Ranges, for which the author reports steeply east dipping mylonite/ultramylonite zones with stretching lineations plunging obliquely toward 025°–040° and southwest directed reverse transport. From the timing point of view and on an even broader scale, a correlation with the 680–630 Ma Miles Orogeny [e.g., *Durocher et al.*, 2003] recognized in the Rudall Province, Western Australia [*Smithies and Bagas*, 1997] could also be possible. However, so far, neither the D5 deformation event of *Clarke* [1992] nor the top-to-west mylonites described above have been studied beyond the stage of collecting isolated observations. In the present study, the top-to-west mylonites are not considered in any further detail, other than to note that a clear differentiation between the two sets of mylonites is possible.

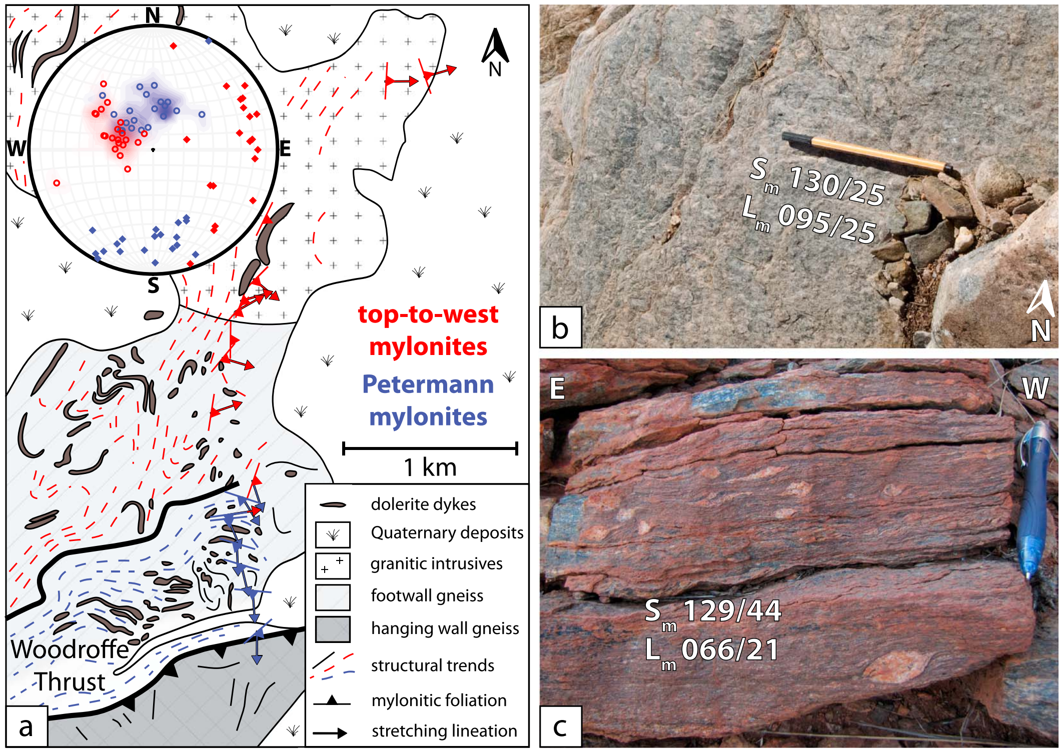

Figure 8. Field data for the top-to-west mylonites, including orientation measurements for the mylonitic foliation (S_m) and stretching lineation (L_m), given as dip direction and dip angle and plunge direction and plunge angle, respectively. (a) Representative measurements of the mylonitic foliation and stretching lineation plotted along a N-S transect into the Woodroffe Thrust (location 13 in Figure 2). Orientation data are plotted in a lower hemisphere Schmidt net, with the mylonitic foliation and stretching lineation represented by poles to planes (open circles) and poles (solid diamonds), respectively. The different kinematics between top-to-west and top-to-north (Petermann) mylonites are apparent. In the footwall, dolerite dykes are folded with roughly NE-SW trending fold axial planes. Folded dolerites and top-to-west mylonites are overprinted by and parallelized into the Woodroffe Thrust mylonites. (b) Field photograph looking down on the mylonitic foliation plane. The stretching lineation (parallel to pen) is almost erased by annealing. Outcrop SW14-193 (coordinates: 131.82563, −26.24933; location 15 in Figure 2). (c) Field photograph of an outcrop plane parallel to the stretching lineation and perpendicular to the mylonitic foliation with sigma clasts indicating top-to-west sense of movement. Outcrop FW14-229 (coordinates: 131.92474, −26.16000; location 13 in Figure 2).

5. Microstructure, Petrography, and Mineral Chemistry

Mylonites and shear zones with Petermann kinematics preserve two distinctly different microstructures, which are referred to as "type A" and "type B" in the following sections and differ with regard to the presence or absence of postkinematic static annealing, respectively (Figure 9). Type-B microstructures still largely preserve pristine, ribbon-like aggregates of quartz and feldspar (Figure 9b), whereas in type A the mylonitic microstructure (Figure 9a), which was presumably once similar to that of type B, is annealed. In locations 14–16 (Figure 2) both microstructural types can be identified, whereas in locations 1–13 (Figure 2), only type B is recognized. With this distinction in mind, felsic and mafic units can be characterized as follows.

5.1. Felsic Assemblages

5.1.1. Mylonites and Shear Zones

Mylonitic granitoids, felsic granulites, and felsic pseudotachylytes have a synkinematic mineral assemblage (decreasing modal abundance from left to right) of Qz + Pl + Kfs + Grt + Bt ± Ilm ± Hbl ± Mag ± Cal. Samples with a type-A microstructure also include clinopyroxene, scapolite, titanite, or epidote, whereas those with a type-B microstructure additionally preserve kyanite, clinopyroxene, or rutile in the south (locations 13–16 in Figure 2) and epidote, muscovite, titanite, or chlorite in the north (locations 1–11 in Figure 2). New garnet is commonly subhedral (Figure 9a), whereas relict garnet is typically fractured (Figure 10a). These fractures are occasionally filled with biotite compositionally identical to the biotite of

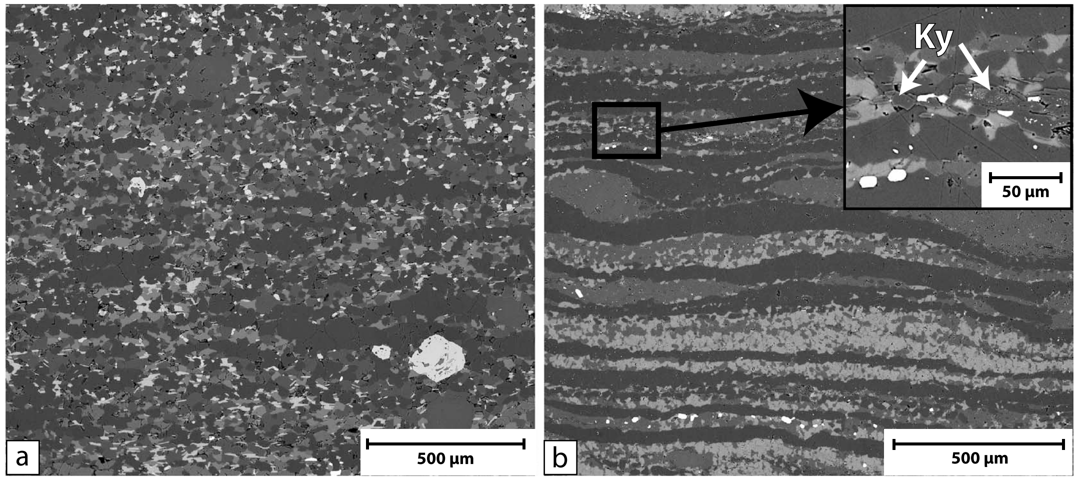

Figure 9. (a) BSE image of a felsic mylonite showing evidence of postkinematic static annealing (type-A microstructure). Mineral assemblage is Qz + Pl + Kfs + Bt + Scp + Hbl + Grt + Ilm + Ep + Cal. Thin section is oriented N-S (left-right). Sample SW13-125 (coordinates: 131.87338, −26.20470; location 14 in Figure 2). (b) BSE image of a felsic mylonite lacking evidence of postkinematic static annealing (type-B microstructure). Mineral assemblage is Qz + Pl + Kfs + Grt + Ky + Bt + Ilm. Thin section is oriented N-S (left-right). Plagioclase clasts indicate a sinistral sense of shear, consistent with top-to-north thrusting. Sample SW13-161 (coordinates: 131.77445, −26.30759; location 16 in Figure 2).

the mylonitic matrix. Fibrous kyanite (Figure 9b), attributed to the high-pressure plagioclase breakdown reaction An = Grs + Ky + Qz [*Boyd and England*, 1961; *Hariya and Kennedy*, 1968], has been identified by Raman spectroscopy and EBSD (supporting information B). Rare isolated shear zones showing top-to-south kinematics preserve the same high-grade mineral assemblage as the Woodroffe Thrust mylonites. Chlorite has only been observed once (location 11 in Figure 2). Relict minerals, presumably developed during the Musgravian Orogeny, include Pl, Kfs, Grt, Cpx, Opx, Qz, Bt, Ep, Hbl, Ilm, Mag, Ttn, Scp, Sill, and Zrn.

Within a single sample, the composition of synkinematically crystallized mineral phases is rather uniform (Figure 11). Garnet has the approximate composition $Fe_{55\text{-}60}Mg_{10\text{-}15}Ca_{20\text{-}25}Mn_{5\text{–}10}$ in type-A microstructures. At similar latitude, garnet in type-B microstructures is typically 5–10% poorer in almandine and 10–20% richer in pyrope component, whereas toward the northernmost locations the spessartine component progressively increases to 10–25% with a corresponding decrease in pyrope component down to ~5%. Recrystallized plagioclase ranges in composition from albite to oligoclase with a trend toward sodium-richer composition when moving from south to north. Relict plagioclase has oligoclase to andesine composition, i.e., richer in anorthite component than recrystallized grains within the same sample. K-feldspar clasts and recrystallized grains are almost pure orthoclase showing no apparent compositional trend across the field area. Recrystallized clinopyroxene has the composition of diopside with an average jadeite component of ~8%.

Wavelength-dispersive X-ray spectroscopy mapping of large garnet clasts in felsic samples with a type-B microstructure (Figure 10) revealed zoning patterns that reflect three different garnet compositions (Figures 10b and 10c). Relict lower-calcium cores (Grt 1a) show a progressive transition into higher-calcium rims (Grt 1b and Grt 2). Grt 1b and Grt 2 are compositionally very similar, but Grt 2 is slightly poorer in calcium and richer in magnesium than Grt 1b (Figure 10d). Diffusion rims along cracks are apparent. Previous work of *Camacho et al.* [2009], in the hanging wall of the Woodroffe Thrust, has interpreted lower-calcium garnet to be related to the Musgravian Orogeny, whereas smaller newly grown higher-calcium garnet and calcium-enriched rims on relict garnet were attributed to the Petermann Orogeny. Based on this, we also consider Grt 1 to be Musgravian and preserved without modification as Grt 1a, while Grt 1b was modified by diffusion early in the Petermann Orogeny and subsequently overgrown by neo-crystallized Petermann-aged Grt 2. Grt 2 rims are very narrow where they overgrew relict garnet, in comparison to the size of newly grown small grains of Grt 2 (lower third of Figures 10b and 10c).

5.1.2. Static Overprint in the Surrounding Country Rock

Samples from low-strain domains, lacking any discernible dynamic Petermann overprint, reveal petrographic features directly comparable to those within adjacent mylonites and isolated shear zones, namely (1)

10.1002/2017TC004681

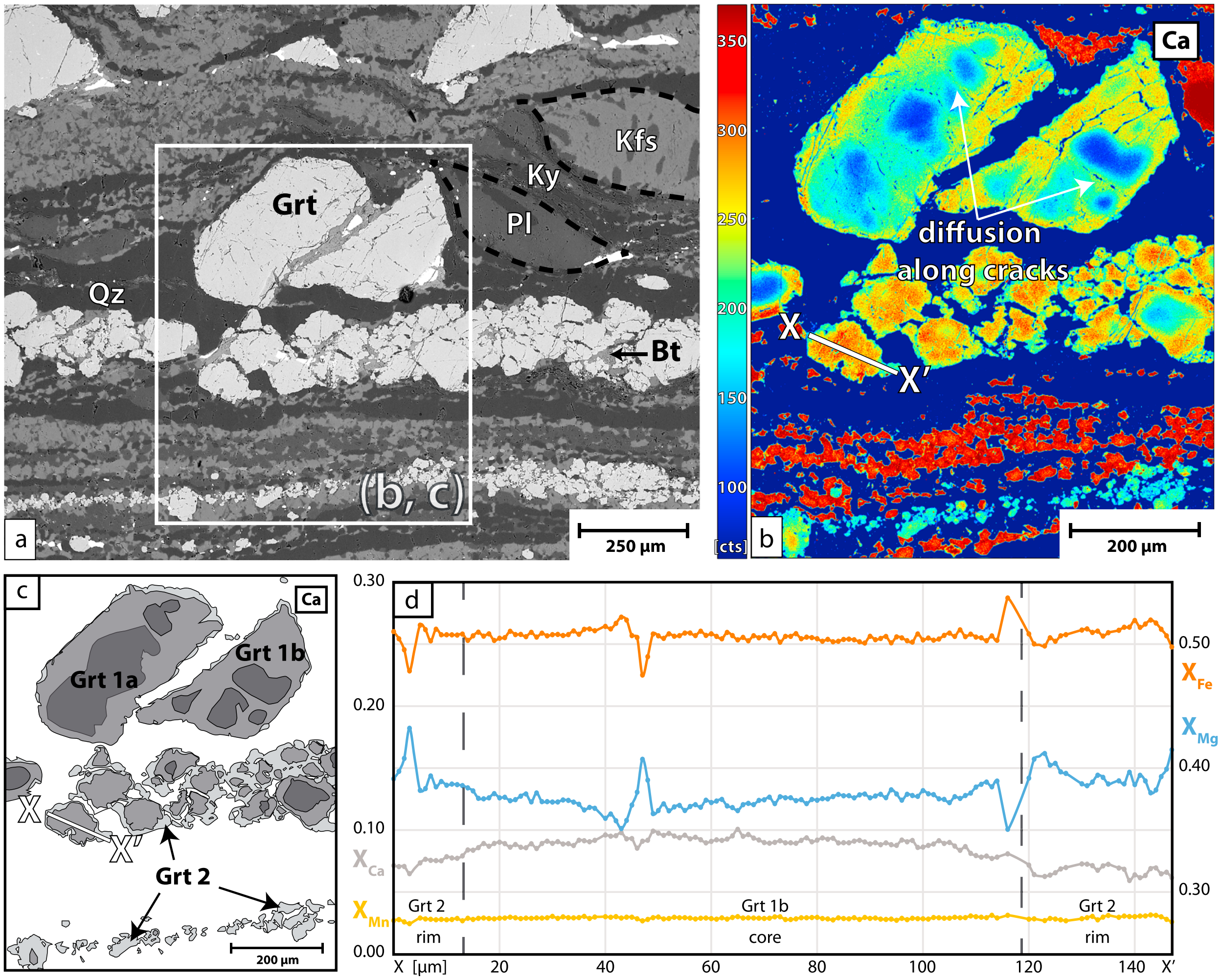

Figure 10. Felsic mylonite with a type-B microstructure. Stable mineral assemblage is Qz + Pl + Kfs + Grt + Bt + Ky + Ilm. Thin section is oriented N-S (left-right). Relict garnet is fractured and filled with biotite. Sample SW13-161 (coordinates: 131.77445, −26.30759; location 16 in Figure 2). (a) BSE image. Sigmoidal plagioclase and K-feldspar clasts indicate a sinistral sense of shear, consistent with top-to-north thrusting. (b) Calcium map. Diffusion rims along cracks are apparent. (c) Sketch of calcium map. Three different garnet compositions are distinguished (Grt 1a, Grt 1b, and Grt 2). (d) Compositional profile X- X′ across a garnet grain with Grt 1b core and Grt 2 rim.

neo-crystallized calcium-rich garnet, (2) kyanite inclusions in plagioclase, and (3) zoned garnet clasts with higher-calcium rims and lower-calcium cores (supporting information C). Mineral chemistry is equivalent to that of nearby dynamically recrystallized samples (Figure 11).

5.2. Mafic Assemblages

5.2.1. Mylonites and Shear Zones

In the southern locations (13–16 in Figure 2), dynamically recrystallized dolerite dykes and associated pseudotachylytes preserve a synkinematic mineral assemblage (decreasing modal abundance from left to right) of Pl + Cpx + Grt + Ilm ± Rt ± Ky ± Qz ± Kfs ± Hbl ± Bt, with the amount of newly grown garnet gradually decreasing toward the north. Samples with type-A microstructure are occasionally complemented by scapolite, whereas those with type-B microstructure additionally preserve orthopyroxene, magnetite, or calcite. Relict minerals include clinopyroxene, orthopyroxene, and plagioclase. In the northernmost locations (1–11 in Figure 2) garnet is absent, samples show a greenschist facies assemblage of Pl + Bt + Act + Chl + Ilm + Qz + Ttn ± Hbl ± Mag, and plagioclase has fractured rather than dynamically recrystallized.

Within a single sample, the composition of synkinematic mineral phases is uniform (Figure 12). Garnet has a slightly higher pyrope component than in the felsic units, with compositions varying between

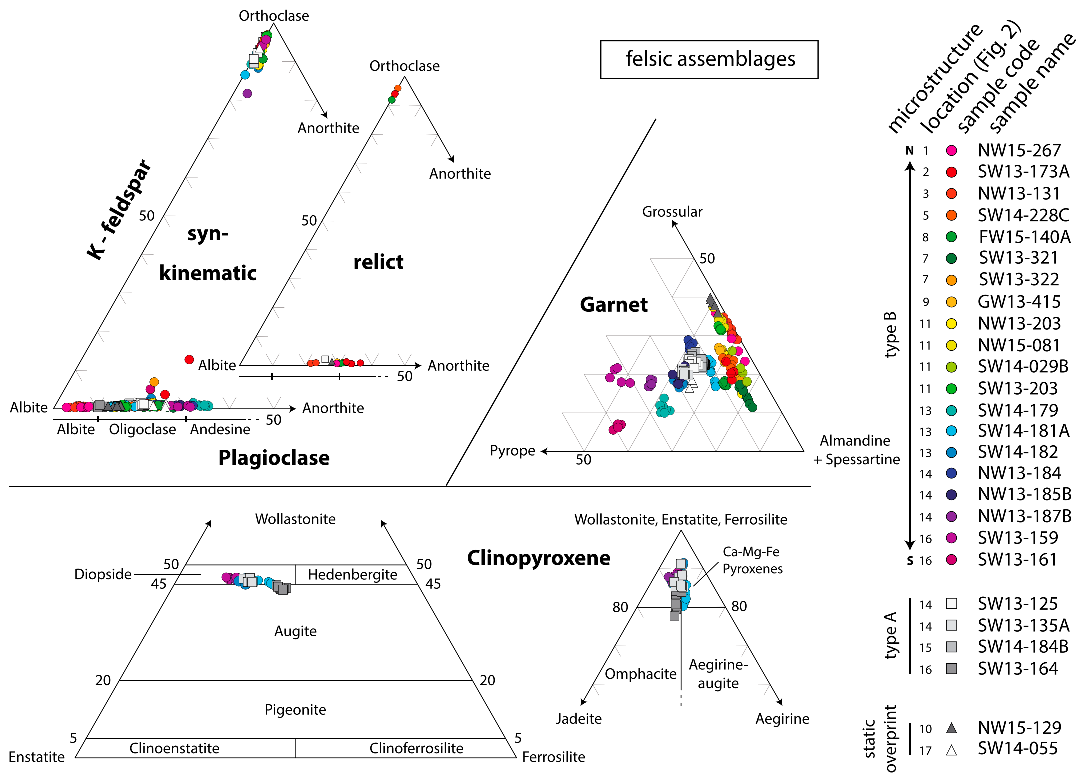

Figure 11. Mineral chemistry of felsic assemblages (Woodroffe Thrust, central Musgrave Block).

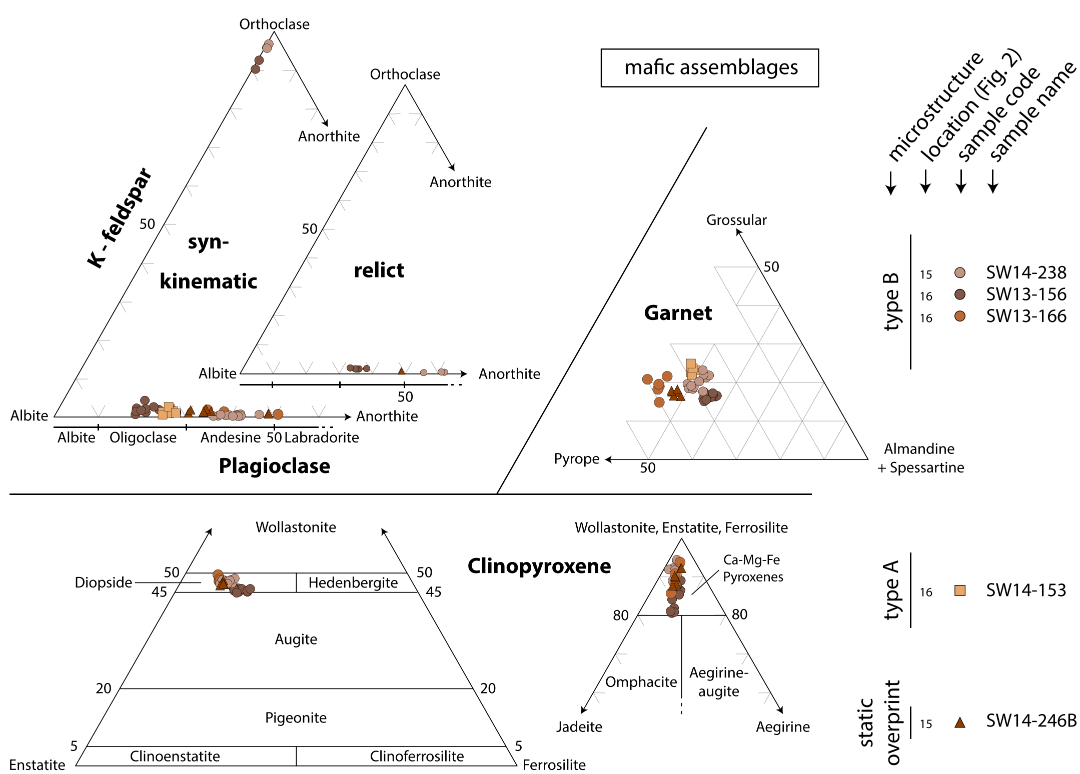

Figure 12. Mineral chemistry of mafic assemblages (Woodroffe Thrust, central Musgrave Block).

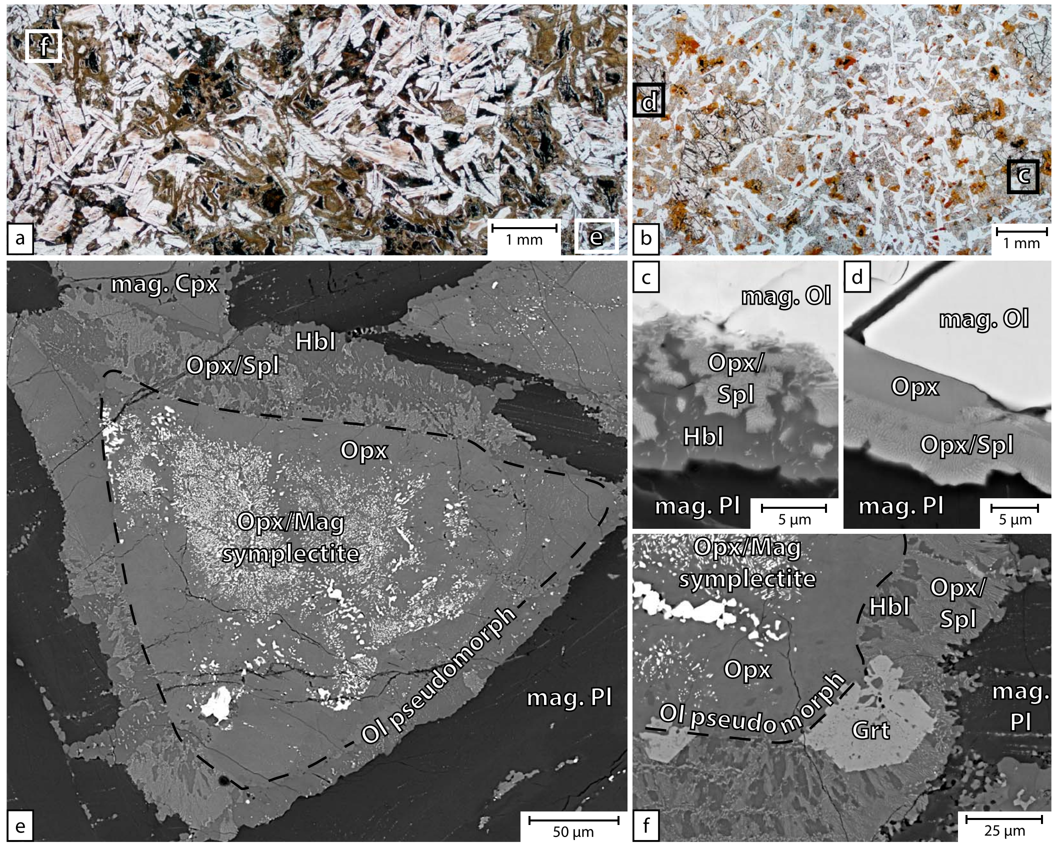

Figure 13. Alcurra Dolerite from (a) footwall and (b) hanging wall of the Woodroffe Thrust with an original magmatic (mag.) fabric but metamorphic assemblage. (a) Unoriented thin section with preserved magmatic Pl + Cpx and metamorphic Opx + Spl + Hbl + Grt + Mag under plane-polarized light. Sample NW14-423B (coordinates: 131.84368, −26.11423; location 12 in Figure 2). (b) Unoriented thin section with preserved magmatic Pl + Cpx + Ol + Ilm and metamorphic Cpx + Opx + Mag + Spl + Bt + Hbl under plane-polarized light. Sample SW14-014 (coordinates: 131.71750, −26.00870; location 11 in Figure 2). (c, d) BSE images of Hbl-Opx/Spl symplectite and Opx/Spl symplectite-Opx coronas between magmatic plagioclase and olivine. (e, f) BSE images of Hbl-Opx/Spl symplectite coronas between magmatic plagioclase and Opx/Mag symplectite-Opx pseudomorphs after olivine, occasionally overgrown by neo-crystallized garnet (Figure 13f).

$Fe_{45}Mg_{25-30}Ca_{20-25}Mn_5$ in type-A microstructures and $Fe_{40-55}Mg_{25-40}Ca_{15-25}Mn_5$ in type-B microstructures. Recrystallized plagioclase has a higher anorthite content compared to felsic units at similar latitude. Relict plagioclase clasts range in composition from andesine to labradorite and are typically between 15 and 20% more calcic than recrystallized grains within the same sample. Similar to the felsic units, recrystallized K-feldspar is almost pure orthoclase and shows no apparent regional trend, while clinopyroxene recrystallized as diopside with an average jadeite component of ~7%.

5.2.2. Static Overprint in the Surrounding Country Rock

Undeformed dolerite dykes from the hanging wall and footwall of the Woodroffe Thrust still preserve an original magmatic fabric but show a variable metamorphic overprint (Figure 13). Our observations confirm that the primary magmatic mineral assemblage in the Alcurra Dolerite is dominantly Cpx + Pl + Ol + Mag + Ilm with an ophitic to subophitic texture [*Camacho et al*., 1991; *Edgoose et al*., 1993] (Figures 13a and 13b). Within these dykes, magmatic clinopyroxene was partially replaced by orthopyroxene, clinopyroxene, and magnetite. The magmatic plagioclase locally shows corroded grain boundaries and coronas of Hbl-Opx/Spl symplectite-Opx when in contact with magmatic olivine (Figures 13c and 13d) or with Opx/Mag symplectite-Opx pseudomorphs after olivine (Figures 13e and 13f). These coronas are variable in thickness (~10 μm in Figures 13c and 13d and ~50 μm in Figures 13e and 13f) and occasionally overgrown by euhedral new garnet (Figure 13f). Throughout the southern locations (13–16 in Figure 2), neo-crystallized garnet and kyanite inclusions in plagioclase are also common in undeformed dolerite dykes (supporting information D), similar to what is observed in the mafic mylonites.

6. Pressure-Temperature Estimates

Pressures and temperatures have been calculated using conventional thermometers and barometers, taking into account (1) their calibration range, (2) restrictions in terms of mineral chemistry, and (3) the mineral assemblage of our samples. Only those applicable to a large number of samples were selected, in order to assure consistency between the estimates. Applied thermometers include Grt-Cpx [*Krogh Ravna*, 2000] and Grt-Bt [*Perchuk and Lavrent'eva*, 1983; *Holdaway*, 2000], while applied barometers include Grt-Bt-Pl-Qz [*Wu et al*., 2004], Grt-Pl-Cpx-Qz [*Newton and Perkins*, 1982; *Eckert et al*., 1991], and Grt-Pl-Als-Qz [*Newton and Haselton*, 1981; *Holdaway*, 2001]. Ferric iron was calculated by stoichiometry and charge balance for garnet and biotite, and following the procedure of *Droop* [1987] for clinopyroxene. Between 4 and 11 independent mineral pairs were matched for each sample, with SW13-173A and SW13-135A having two separate sets that each refers to different thermobarometers. The number of pairs was reduced for SW13-161, because the mineral composition was partially outside of the calibration range of the Grt-Bt-Pl-Qz barometer [*Wu et al*., 2004]. Pressures and temperatures were determined iteratively and used as the input parameters for the applied thermometers and barometers, respectively. Preferentially, the iteration was done between the Grt-Bt thermometer of *Holdaway* [2000] and the Grt-Pl-Als-Qz barometer of *Holdaway* [2001], as these are considered to be most reliable [*Wu and Cheng*, 2006]. For samples lacking kyanite, either the Grt-Bt-Pl-Qz barometer of *Wu et al*. [2004] or the Grt-Pl-Cpx-Qz barometer of *Newton and Perkins* [1982] was applied for the iteration process. In samples lacking biotite, temperature was determined using the Grt-Cpx thermometer of *Krogh Ravna* [2000]. For comparison on a regional scale, the Grt-Bt thermometer was used, as most samples contain biotite. Where pressure could not be directly estimated (e.g., because mineral chemistry was not within the appropriate calibration range), pressures from comparable samples nearby were used as input to determine temperature. The results are summarized in Table 1 and presented separately for mylonites with (1) type-B microstructure, (2) type-A microstructure, and (3) for statically overprinted samples and isolated shear zones outside of the Woodroffe Thrust mylonitic zone. Representative mineral data are presented in Table 2.

6.1. Mylonites With a Type-B Microstructure

Conventional geothermometry for mylonites with a type-B microstructure yields locally consistent temperature estimates (Table 1). Variations do occur on a larger scale and match the observed gradients in mineral chemistry, with metamorphic grade increasing toward the south. The Grt-Bt thermometer of *Perchuk and Lavrent'eva* [1983] yields average temperatures of ~460°C in the north (locations 1–9 in Figure 2) and ~540°C in the south (locations 13–16 in Figure 2). For the same sample groups, the Grt-Bt thermometer of *Holdaway* [2000] yields higher average temperatures of ~550°C in the north and ~590°C in the south. These results are, where applicable, supported by Grt-Cpx thermometry [*Krogh Ravna*, 2000]. For a particular calibration, systematic uncertainties are the same and their contribution to the final results thereby minimized [*Worley and Powell*, 2000]. Relative differences in calculated temperatures are therefore considered to be reasonably precise and more reliable than absolute values, supporting the interpretation of increasing metamorphic grade toward the south. The slightly higher temperature estimates using the calibration of *Holdaway* [2000] are geologically realistic, because feldspar recrystallization, a process generally considered to be active above 500°C [*Voll*, 1976; *Simpson*, 1985; *Gapais*, 1989], occurred in the mylonites of the Woodroffe Thrust along the entire N-S profile length considered in the current study (Figure 2). Feldspar recrystallization was also reported by *Bell and Johnson* [1989] from the area north of Amata (corresponding to our location 6 in Figure 2). In Figure 14, temperature estimates from *Holdaway* [2000] are plotted against sample latitude to show the spatial variation from north to south. From the northernmost to the southernmost location of the entire ~60 km profile, an increase of only ~100°C (from 520°C to 620°C) is apparent. Although we argue in favor of the absolute values derived from the calibration of *Holdaway* [2000], the calculated temperatures using that of *Perchuk and Lavrent'eva* [1983] also show a similar relative increase from north to south (Table 1).

Results from conventional geobarometry typically range from 0.8 to 1.1 GPa but do not show any obvious regional trend (Table 1). The order of magnitude is in agreement with the reports of newly grown Petermann-aged kyanite in footwall sedimentary rocks farther west in the Petermann Ranges [*Scrimgeour et al*., 1999] and with the fact that the peristerite gap in plagioclase [*Maruyama et al*., 1982] has not been observed in the studied samples. However, estimated pressures are to be considered with some caution for the following two reasons. First, pressures are potentially overestimated by >0.3 GPa, since the product

Table 1
Pressure and Temperature Results Using Conventional Geothermobarometry, Central Musgrave Block[a]

	Location (Figure 2)	Sample Code	Mineral Pairs	Thermometers (°C ± 2σ) Grt-Cpx R00 (± 100 °C)	Grt-Bt PL83 -		Grt-Bt H00 (± 25 °C)		Barometers (GPa ± 2σ) Grt-Bt-Pl-Qz W04 (± 0.12 GPa)	Grt-Pl-Cpx-Qz NP82 (± 0.16 GPa)	Grt-Pl-Cpx-Qz E91 -	Grt-Pl-Als-Qz NH81 (± 0.11 GPa)	Grt-Pl-Als-Qz H01 (± 0.08 GPa)	Geothermal Gradient (°C/km)	
Type-B Microstructure (WT)	1	NW15-267	7	-	411 ± 25		525 ± 25		-	-	-	-	-	-	
	2	SW13-173A	5 (4)	-	493 ± 22		582 ± 17*		0.94 ± 0.10*	-	-	-	-	16,4	
	3	NW13-131	8	-	410 ± 28	Ave. 462 ± 84	512 ± 18	Ave. 555 ± 63	-	-	-	-	-	-	
	5	SW14-228C	6	-	462 ± 50		554 ± 46*		1.02 ± 0.16*	-	-	-	-	14,4	
	7	SW13-321	9	-	468 ± 22		551 ± 14*		0.73 ± 0.12*	-	-	-	-	20,0	
	7	SW13-322	4	-	451 ± 42		546 ± 37*		0.88 ± 0.09*	-	-	-	-	16,4	
	8	FW15-140A	5	-	539 ± 13		613 ± 02*		0.99 ± 0.05*	-	-	-	-	16,4	
	9	GW13-415	4	-	463 ± 08		555 ± 08*		0.93 ± 0.07*	-	-	-	-	15,8	Ave. 16.4
	13	SW14-179	8	-	522 ± 23		547 ± 27		-	-	-	-	-	-	
	13	SW14-181A	7	569 ± 45	446 ± 15		526 ± 09*		-	0.97 ± 0.11*	0.87 ± 0.11	-	-	14,4	
	13	SW14-182	7	508 ± 30	526 ± 11		573 ± 24*		-	0.94 ± 0.10*	0.85 ± 0.10	-	-	16,1	
	14	NW13-184	6	-	552 ± 66	Ave. 542 ± 87	624 ± 58*	Ave. 593 ± 80	1.08 ± 0.22*	-	-	-	-	15,3	
	14	NW13-185B	6	-	582 ± 13		642 ± 07*		0.99 ± 0.13*	-	-	-	-	17,2	
	14	NW13-187B	6	538 ± 32	527 ± 18		582 ± 18*		-	0.96 ± 0.07*	0.89 ± 0.06	-	-	16,1	
	15	SW14-238	11	543 ± 76*	-		-		-	0.79 ± 0.14	0.78 ± 0.13	0.77 ± 0.19	0.80 ± 0.17*	18,0	
	16	SW13-156	11	550 ± 52	571 ± 29		622 ± 21*		-	1.09 ± 0.10	1.02 ± 0.10	1.14 ± 0.20	1.14 ± 0.11*	14,5	
	16	SW13-159	5	573 ± 118	571 ± 56		632 ± 52*		-	1.08 ± 0.21	1.02 ± 0.21	1.09 ± 0.19	1.10 ± 0.20*	15,2	
	16	SW13-161	5 (1)	-	582 ± 22		588 ± 34*		0,80	-	-	0.79 ± 0.07	0.81 ± 0.08*	19,2	
	16	SW13-166	6	595 ± 62*	-		-		-	0.96 ± 0.10	0.98 ± 0.08	0.92 ± 0.13	0.94 ± 0.12*	16,8	
Type-A Microstructure (WT)	14	SW13-125	9	-	598 ± 40	Ave. 576 ± 129	668 ± 31*	Ave. 643 ± 98	1.13 ± 0.07*	-	-	-	-	15,7	
	14	SW13-135A	8 (3)	574 ± 31*	625 ± 21		682 ± 12		-	1.11 ± 0.07*	1.01 ± 0.08	-	-	13,7	
	15	SW14-184B	8	-	511 ± 16		590 ± 13		-	-	-	-	-	-	
	16	SW13-153	7	-	641 ± 17		686 ± 10		-	-	-	-	-	-	
	16	SW13-164	8	633 ± 31*	504 ± 12		590 ± 11		-	1.33 ± 0.04*	1.24 ± 0.04	-	-	12,6	
Static overprint	11 (HW)	NW15-129	7	-	434 ± 10		526 ± 10		-	-	-	-	-	-	
	15 (HW)	SW14-246B	6	493 ± 57*	-		-		-	0.82 ± 0.11	0.80 ± 0.10	0.70 ± 0.15	0.73 ± 0.13*	21,5	
	17 (FW)	SW14-055	6	-	556 ± 16		624 ± 26*		1.07 ± 0.11	-	-	1.06 ± 0.11	1.08 ± 0.12*	15,3	
Isolated shearing (Figure 7b top)	11 (HW)	NW13-203	8	-	475 ± 33		517 ± 49*		0.87 ± 0.13*	-	-	-	-	15,7	
	11 (HW)	NW15-081	9	-	463 ± 31		545 ± 22		-	-	-	-	-	-	
Isolated shearing (Figure 7b bottom)	11 (HW)	SW14-029B	5	-	461 ± 14		551 ± 08*		0.97 ± 0.16*	-	-	-	-	15,0	
	11 (HW)	SW13-203	6	-	469 ± 21		553 ± 18		-	-	-	-	-	-	

[a]Samples are grouped according to microstructure and structural position: WT = Woodroffe Thrust mylonitic zone, FW = footwall, HW = hanging wall. Applied thermometers: R00 = *Krogh Ravna* [2000], PL83 = *Perchuk and Lavrent'eva* [1983], H00 = *Holdaway* [2000]. Applied barometers: W04 = *Wu et al.* [2004], NP82 = *Newton and Perkins* [1982], E91 = *Eckert et al.* [1991], NP81 = *Newton and Haselton* [1981], H01 = *Holdaway* [2001]. Calibrations used for iterative determination of pressure and temperature are indicated by an asterisk (*). Statistical variability is expressed as 2 times standard deviation (2σ). Absolute uncertainties for each calibration are given in brackets. Sample descriptions are given in the supporting information E. Ave = average.

of X_{Grs} in garnet and X_{An} in plagioclase is often <0.05 [*Todd*, 1998] and mineral chemistry sometimes straddles the calibration limits of the applied Grt-Bt-Pl-Qz barometer [*Wu et al.*, 2004]. We were careful to ensure that the respective calibration limits were not exceeded for the results listed in Table 1. Second, for all our samples, estimated pressures fall within the kyanite stability field [*Holdaway*, 1971], which is in contrast to previous reports of relict (presumably Musgravian-aged) sillimanite locally preserved in undeformed footwall and hanging wall rocks in the general area of the northern study locations [*Wilson and Hudson*, 1967; *Camacho and Fanning*, 1995]. This apparent contradiction is commonly observed in polymetamorphic terranes and is potentially explained by the ability of metastable Al_2SiO_5 polymorphs to persist outside their stability field without any signs of transformation, as a consequence of sluggish reaction rates [*Fyfe et al.*, 1978; *Winkler*, 1979].

6.2. Mylonites With a Type-A Microstructure

Mylonites with a type-A microstructure are restricted to the southern region and typically record the highest metamorphic conditions (Table 1). Grt-Bt thermometry yields average temperatures of ~580°C using the calibration of *Perchuk and Lavrent'eva* [1983] and ~640°C with that of *Holdaway* [2000]. In both cases, calculated temperatures are notably higher than those estimated for mylonites with a type-B microstructure (Table 1). This difference is likely to be geologically meaningful, since relative differences in calculated temperatures

Table 2
Representative Mineral Data for Recrystallized Felsic and Mafic Assemblages in the Central Musgrave Block

Garnet

Sample	SW13-173A	SW13-156	SW13-161	SW13-135A	SW14-55	SW14-029B
EMPA point	3707	2632	2135	3780	1828	3522
SiO_2	37,64	38,78	39,47	37,99	37,64	37,17
TiO_2	0,17	0,06	0,06	0,13	0,07	0,10
Al_2O_3	21,36	22,16	22,35	21,65	22,14	21,48
FeO_{total}	24,37	25,61	24,62	26,30	26,98	26,75
MnO	8,24	0,71	1,28	2,24	2,51	4,55
MgO	1,43	7,19	10,44	4,50	4,68	0,83
CaO	7,15	6,04	2,29	7,13	6,55	9,04
Na_2O	0,02	0,00	0,01	0,00	0,00	0,02
K_2O	0,06	0,01	0,06	0,10	0,02	0,04
Total	100,44	100,56	100,58	100,04	100,59	99,98
Structural Formulae Based On 12 Oxygens						
T Si	3,00	2,98	2,99	2,98	2,95	2,98
T Al	0,00	0,02	0,01	0,02	0,05	0,02
M1 Al	2,01	1,99	1,99	1,99	1,99	2,01
M1 Fe	0,00	0,00	0,00	0,00	0,00	0,00
M1 Ti	0,01	0,00	0,00	0,01	0,00	0,01
M2 Fe	1,62	1,65	1,56	1,73	1,77	1,79
M2 Mg	0,17	0,82	1,18	0,53	0,55	0,10
M2 Ca	0,61	0,50	0,19	0,60	0,55	0,78
M2 Mn	0,56	0,05	0,08	0,15	0,17	0,31
Alm	0,55	0,55	0,52	0,58	0,58	0,60
Prp	0,06	0,27	0,39	0,18	0,18	0,03
Grs	0,21	0,17	0,06	0,20	0,18	0,26
Sps	0,19	0,02	0,03	0,05	0,05	0,10

Biotite

Sample	SW13-173A	SW13-156	SW13-161	SW13-135A	SW14-55	SW14-029B
EMPA point	3722	2623	2134	1667	1832	3530
SiO_2	36,41	36,39	38,60	35,34	36,05	35,92
TiO_2	2,14	3,68	3,98	3,23	2,51	3,64
Al_2O_3	17,02	15,86	15,09	14,89	17,85	16,57
FeO_{total}	19,96	11,78	9,23	18,78	14,43	21,44
MnO	0,10	0,03	0,00	0,16	0,16	0,10
MgO	10,25	17,44	18,13	12,61	13,84	7,38
CaO	0,23	0,07	0,09	0,19	0,09	0,02
Na_2O	0,19	0,04	0,11	0,03	0,01	0,01
K_2O	9,10	10,01	9,88	9,11	9,35	9,81
Total	95,41	95,29	95,11	94,34	94,29	94,89
Structural Formulae Based On 11 Oxygens						
Si	2,77	2,69	2,81	2,73	2,71	2,78
Al (IV)	1,23	1,31	1,19	1,27	1,29	1,22
Ti	0,12	0,20	0,22	0,19	0,14	0,21
Al (VI)	0,30	0,07	0,10	0,08	0,29	0,30
Fe	1,27	0,73	0,56	1,21	0,91	1,39
Mn	0,01	0,00	0,00	0,01	0,01	0,01
Mg	1,16	1,92	1,97	1,45	1,55	0,85
Ca	0,02	0,01	0,01	0,02	0,01	0,00
Na	0,03	0,01	0,02	0,00	0,00	0,00
K	0,88	0,94	0,92	0,90	0,90	0,97

Plagioclase

Sample	SW13-173A	SW13-156	SW13-161	SW13-135A	SW14-55	SW14-029B
EMPA point	3697	2652	2136	3795	1876	3538
SiO_2	62,74	63,28	62,28	63,68	62,69	63,46
TiO_2	0,02	0,05	0,07	0,05	0,03	0,04
Al_2O_3	23,27	23,61	23,27	21,93	24,48	22,62
FeO_{total}	0,19	0,21	0,21	0,23	0,08	0,14
MnO	0,00	0,01	0,00	0,04	0,00	0,00
MgO	0,03	0,00	0,00	0,00	0,00	0,00
CaO	4,36	3,95	4,23	3,10	4,42	3,37
Na_2O	8,55	8,50	8,61	9,37	8,45	9,29
K_2O	0,13	0,22	0,15	0,15	0,13	0,10
Total	99,28	99,83	98,83	98,55	100,28	99,02
Structural Formulae Based On 8 Oxygens						
Si	2,79	2,79	2,78	2,85	2,76	2,82
Ti	0,00	0,00	0,00	0,00	0,00	0,00
Al	1,22	1,23	1,23	1,16	1,27	1,19
Fe	0,01	0,01	0,01	0,01	0,00	0,01
Mn	0,00	0,00	0,00	0,00	0,00	0,00
Mg	0,00	0,00	0,00	0,00	0,00	0,00
Ca	0,21	0,19	0,20	0,15	0,21	0,16
Na	0,74	0,73	0,75	0,81	0,72	0,80
K	0,01	0,01	0,01	0,01	0,01	0,01
X_{Ab}	0,77	0,78	0,78	0,84	0,77	0,83
X_{An}	0,22	0,20	0,21	0,15	0,22	0,17
X_{Or}	0,01	0,01	0,01	0,01	0,01	0,01

Clinopyroxene

Sample	SW13-156	SW13-135A
EMPA point	2656	3784
SiO_2	51,89	52,53
TiO_2	0,28	0,16
Al_2O_3	5,31	2,67
FeO_{total}	8,75	9,31
MnO	0,06	0,18
MgO	11,56	11,91
CaO	18,83	20,83
Na_2O	2,58	1,66
K_2O	0,06	0,10
Total	99,31	99,35
Struct. Form. Based On 6 Oxygens		
T Si	1,94	1,97
T Al	0,06	0,03
Mn	0,00	0,01
Ca	0,75	0,84
Al	0,23	0,12
Mg	0,64	0,67
Ti	0,01	0,00
Al	0,17	0,09
Fe^{2+}	0,17	0,22
Fe^{3+}	0,10	0,08
Na	0,19	0,12
En	0,39	0,37
Fs	0,16	0,16
Wo	0,45	0,47
Wo/En/Fs	0,81	0,88
Jd	0,12	0,07
Aeg	0,07	0,06

Sample	Description	Information	Location (Figure 2)
SW13-173A	mylonitized felsic gneiss	type-B microstructure	2 (WT)
SW13-156	mylonitized dolerite dyke	type-B microstructure	16 (WT)
SW13-161	mylonitized felsic gneiss	type-B microstructure	16 (WT)
SW13-135A	mylonitized felsic gneiss	type-A microstructure	14 (WT)
SW14-055	felsic gneiss	static overprint	17 (FW)
SW14-029B	sheared granite	isolated shearing	11 (HW)

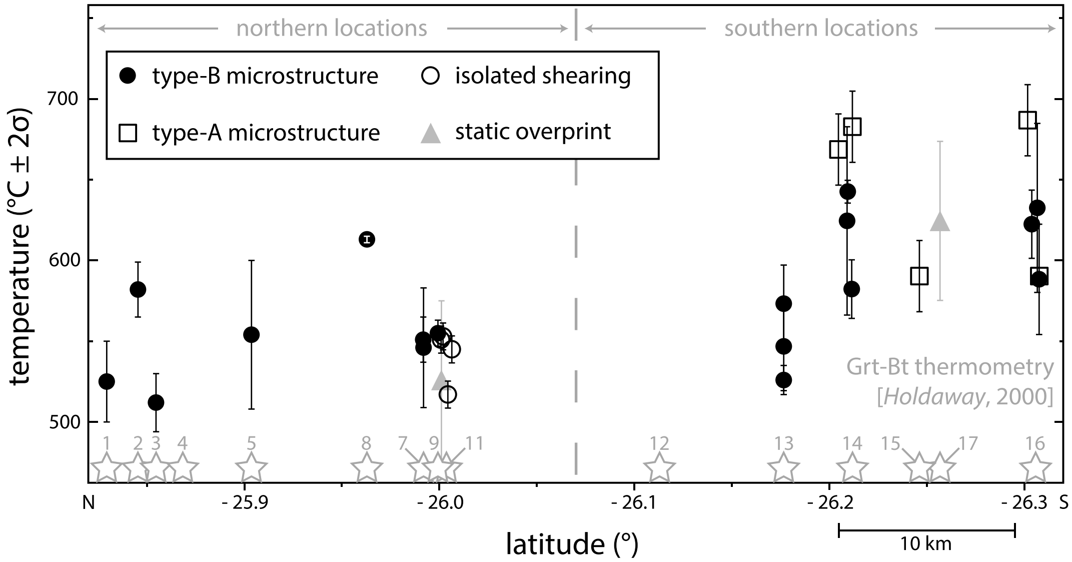

Figure 14. Regional variation in microstructure and temperature estimates plotted against sample latitude. Bars represent statistical variability. Calibration uncertainties are not included, as these would be the same for all samples. The studied locations (see Figure 2) are indicated. Data are given in Table 1.

are constrained reasonably precisely within each calibration [*Worley and Powell*, 2000]. Pressures are also slightly higher (1.0 to 1.3 GPa) than in the mylonites with type-B microstructure.

The two microstructural types are structurally related, with type A and type B occurring at the periphery and in the interior of the Woodroffe Thrust mylonitic zone, respectively (Figure 15). From Figure 15 it is evident that reconstructed metamorphic conditions generally decrease toward the more internal parts of the shear zone, consistent with the shift from type-A to type-B microstructures.

6.3. Static Overprint and Isolated Shearing

At similar latitude, metamorphic conditions determined for statically and dynamically recrystallized samples are, within error, identical to one another (Table 1 and Figure 14). Similarly, pressure and temperature

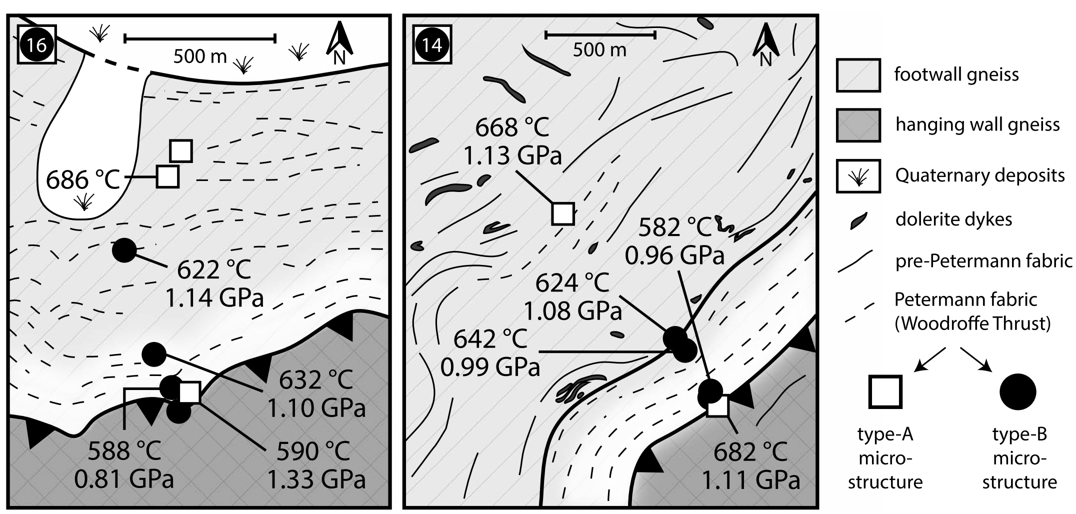

Figure 15. Geographical distribution of mylonitic samples with type-A and type-B microstructures within the southern locations 16 and 14 (see Figure 2 for locations). Plotted temperatures are from Grt-Bt thermometry [*Holdaway*, 2000], while plotted pressures are from Grt-Bt-Pl-Qz barometry [*Wu et al*., 2004], Grt-Pl-Cpx-Qz barometry [*Newton and Perkins*, 1982], or Grt-Pl-Als-Qz barometry [*Holdaway*, 2001]. Data are given in Table 1.

estimates for isolated shear zones in the hanging wall and footwall are, within error, identical to those for the main Woodroffe Thrust mylonites (Table 1 and Figure 14).

The reaction coronas between olivine and plagioclase described in section 5.2.2 are well-known and commonly found in metamorphosed gabbros from medium- to high-grade terranes [*Gardner and Robins*, 1974; *Kretz et al*., 1989]. The observed sequence Ol-Opx-Opx/Spl symplectite-Hbl-Pl (Figures 13c and 13d) has been attributed to the fluid-assisted reaction: Ol + Pl = Opx + Hbl + Spl [*van Lamoen*, 1979; *Kretz et al*., 1989]. Where magmatic olivine is not preserved, it is replaced by Opx/Mag symplectite-Opx pseudomorphs (Figures 13e and 13f), as a result of the fluid-assisted replacement reaction Ol = Opx + Mag [*van Lamoen*, 1979]. These solid-state reactions span a wide field, ranging from amphibolite to granulite facies metamorphism [e.g., *Gardner and Robins*, 1974; *Nishiyama*, 1983; *Kretz et al*., 1989; *Claeson*, 1998], and thus include the metamorphic conditions reconstructed for the Woodroffe Thrust (Table 1). A compilation of reaction boundaries for the olivine-plagioclase versus the spinel-pyroxene system [*Gardner and Robins*, 1974, Figure 1] also supports this conclusion. In addition, the static recrystallization of clinopyroxene, orthopyroxene, and magnetite, as well as the neo-crystallization of garnet, are consistent with the petrographic observations made in the dynamically recrystallized dolerite dykes. It is thus highly unlikely that the coronas structures are simply due to postintrusional magmatic cooling. These observations instead argue that the observed reactions occurred in response to ambient metamorphic conditions during shearing along the Woodroffe Thrust.

7. Discussion

7.1. Metamorphic Conditions

Pressure and temperature calculations on the mineral assemblages of mylonites from the Woodroffe Thrust correspond to high-pressure amphibolite to subeclogite facies conditions and are higher grade than previously reported [*Maboko et al*., 1992; *Camacho and Fanning*, 1995]. The observation that plagioclase and K-feldspar dynamically recrystallized in all the mylonitic samples is consistent with estimated metamorphic temperatures above 500°C. In general, the current exposure level of the Woodroffe Thrust in the study area is characterized by a remarkable lack of retrogression and preserves mineral assemblages and microstructures typical of a deep midcrustal shear zone. The one exception to this general observation are the northernmost dolerite dykes. Although surrounded by high-grade felsic mylonites, these dykes show a pervasive, greenschist facies mineral assemblage, reflecting later hydration and retrogression presumably during exhumation.

Camacho et al. [2001] suggested that the Davenport and North Davenport Shear Zones in the hanging wall of the Woodroffe Thrust experienced a different thermal regime to that in the surrounding country rocks. Assemblages from localized shear zones that formed during the Petermann Orogeny at circa 560–520 Ma indicate synkinematic conditions of circa 650°C and 1.2 GPa [*Ellis and Maboko*, 1992; *Camacho et al*., 1997]. In the undeformed rocks outside these shear zones, minerals with low closure temperatures, such as biotite, preserve $^{40}Ar/^{39}Ar$ and Rb/Sr ages >800 Ma, leading *Camacho et al*. [2001] to the conclusion that the country rocks did not experience temperatures greater than ~450°C for any extended period of time during the Petermann Orogeny. In contrast, the current study demonstrates that metamorphic assemblages related to the Petermann Orogeny are directly comparable in strongly and effectively undeformed units, although the degree of transformation is markedly different, generally being only partially to weakly developed outside the shear zones. Features observed both in dynamically recrystallized mylonites and in statically overprinted felsic and mafic rocks include (1) higher-calcium rims on relict garnet clasts (Figure 10; supporting information C), (2) neo-crystallized garnet (Figures 9a and 13f; supporting information C and D), and (3) kyanite inclusions in plagioclase (Figure 9b; supporting information C and D). The chemistry of neo-crystallized minerals in low- and high-strain domains is also directly comparable (Figures 11 and 12), and the metamorphic conditions determined for dynamically and statically recrystallized samples are similar (Table 1 and Figure 14). Subhedral garnet grains indicate that the metamorphic conditions at least partially outlasted the deformation (Figure 9a). These new observations establish that the P-T conditions presented in Table 1 were in fact ambient and experienced by all units, not just the higher-strain shear zones. In the footwall of the Woodroffe Thrust, this is also in agreement with the near total resetting of $^{40}Ar/^{39}Ar$ ages in pre-Petermann biotite and K-feldspar [*Maboko et al*., 1992] and the static metamorphic overprint in undeformed dolerite dykes (Figure 13).

Having concluded that the determined metamorphic conditions are ambient, geothermal gradients can be calculated. Assuming an average density of 2.7 g/cm^3 for the dominantly quartzo-feldspathic rocks of the central Musgrave Block yields an average of ~16°C/km for samples with type-B microstructure and slightly lower values for those with a type-A microstructure (Table 1). Similar estimates of 16–18°C/km and 17°C/km were obtained from the Davenport Shear Zone in the hanging wall of the Woodroffe Thrust [*Camacho et al*., 1997] and in the Mann Ranges farther west [*Scrimgeour and Close*, 1999], indicating that there was little to no thermal perturbation between hanging wall and footwall. A geothermal gradient of ~17°C/km is low compared to typical values of 25–40°C/km in continent-continent collisional settings [*Gordon et al*., 2012] but is in the typical range for old stable continental crust [*Sclater et al*., 1980]. Similar values of 15–22°C/km would also be predicted for steady state in the middle to lower crust of the central Musgrave Block today, calculating with a current surface heat flow of 65 mW m^{-2} [*McLaren et al*., 2003], a crustal thickness of 50 km [*Aitken et al*., 2009a], a representative Moho temperature of 725°C, and an average crustal conductivity of 3 W/mK [*Cho et al*., 2009].

7.2. Shearing History

Mylonites with type-A microstructure yield notably higher metamorphic conditions (~650°C and 1.0–1.3 GPa) than those with type-B microstructure (ranging between circa 520–620°C and 0.8–1.1 GPa). These textural and metamorphic differences support the idea that the two fabrics represent different time slices during shearing along the Woodroffe Thrust at lower crustal (type-A microstructure) and midcrustal (type-B microstructure) conditions, respectively. Pressures and temperatures estimated for samples with a type-A microstructure are very similar to those determined for the lower crustal Davenport Shear Zone (650°C and 1.2 GPa) in the hanging wall of the Woodroffe Thrust [*Ellis and Maboko*, 1992; *Camacho et al*., 1997] and suggest a contemporaneous development. The northern locations 1–13 (Figure 2) never show a type-A microstructure associated with the Woodroffe Thrust, indicating that, in these locations, the footwall was not at lower crustal level during the Petermann Orogeny. Toward the more southerly exposures (locations 14–16 in Figure 2), which represent progressively deeper crustal levels, both fabrics are preserved. We conclude that the associated high-strain microstructure at the peripheries of the Woodroffe Thrust formed during early lower crustal shearing and annealed (type-A microstructure) as deformation progressively localized into the interior of the mylonitic zone. These internal parts of the Woodroffe Thrust are thus interpreted to record the younger, midcrustal time slice (type-B microstructure). The transition between the two zones is gradual, as is apparent in the progressive shift toward lower metamorphic conditions when moving from the periphery to the interior of the Woodroffe Thrust mylonitic zone (Figure 15). The same transition is preserved petrologically in the higher-calcium overgrowths on relict garnet clasts, reflected in the compositional shift from Grt 1b to the slightly calcium-poorer Grt 2 (Figure 10).

7.3. Geometry

Following the approach of *Cooper et al*. [2010], it is possible to derive the syndeformational geometry of a fault based on the regional variation in coeval ambient metamorphic conditions. Along the Woodroffe Thrust, the shearing history preserved in the older lower crustal type-A microstructures and younger midcrustal type-B microstructures could potentially be used to reconstruct the thrust's geometry at lower crustal and midcrustal depth, respectively. However, samples with a type-A microstructure are limited to a very small part of the study area (locations 14–16 in Figure 2), whereas samples with a type-B microstructure span the entire length of the ~60 km long N-S transect. The following calculations and discussions are therefore only based on the latter samples and focus on the syndeformational geometry of the Woodroffe Thrust at midcrustal level, assuming that the preserved metamorphic conditions in all samples with a type-B microstructure formed coevally. However, even if type-B microstructures in the north were coeval with type-A microstructures in the south, the results would not be altered significantly, as temperature differences between type-A and type-B microstructures in the south are small (<50°C).

From north to south, temperature estimates along the ~60 km profile range from circa 520°C to 620°C (Figure 14), with no discernable variation along strike (i.e., E-W). Values are relatively constant throughout the northern locations but increase toward the south, indicating either a flat ramp or a low-angle ramp geometry that steepens in its southern exposures. We prefer not to overly emphasize the results from the single location 13 (Figure 2) and argue in favor of a low-angle ramp geometry, as this is in agreement with the progressive N-S changes in plagioclase chemistry (Figures 11 and 12) and quartz crystallographic preferred orientation (not presented in the current paper). Over the entire profile, this translates into an average horizontal gradient of only 2°C/km in the direction of thrusting. For an average geothermal gradient of ~16°C/km (Table 1), this regional gradient implies that the Woodroffe Thrust was originally flat lying to shallowly south dipping with an average estimated angle of ≤6°. These calculations do not consider the effects of any potential paleotopography present during the Petermann Orogeny, which was almost certainly higher in the hinterland than in the foreland, reflecting an expected orogenic wedge geometry [e.g., *Platt*, 1986]. The reconstructed geometry requires a displacement along the thrust plane of ~60 km in the direction of thrusting in order to account for the lateral distance between the northernmost outcrop of the granulite facies hanging wall (location 1 in Figure 2) and the southernmost outcrop of the upper amphibolite facies footwall (location 16 in Figure 2). Similar values of shortening (~60 km to >100 km) have been estimated by *Lambeck and Burgess* [1992], *Hand and Sandiford* [1999], and *Flottmann et al*. [2004] based on teleseismic traveltime anomalies, estimated metamorphic conditions of juxtaposed units, and restored cross sections, respectively. The geometrical reconstruction demonstrates that basement-cored, thick-skinned, midcrustal thrusts can define very shallow-dipping and even flat-lying, large-scale features, with dimensions on the order of many of tens of kilometers, before they steepen into the lower crust.

Within the error ranges of conventional geothermobarometry, we do not observe any marked jump in temperature across the Woodroffe Thrust, as can be seen, for example, from a comparison of the results from locations 9 (555°C and 0.93 GPa) and 11 (517–553°C and 0.87–0.97 GPa). This indicates that the Woodroffe Thrust was at least partially thermally reequilibrated during [*Ruppel and Hodges*, 1994] or after [*England and Thompson*, 1984] relative displacement. However, full thermal equilibration after thrust activity is unlikely because type-B deformation microstructures are still preserved along the length of the profile, whereas earlier, annealed type-A microstructures are only observed in the originally deeper and warmer southern samples. If the hanging wall was overthrusted onto a ramp-flat geometry defined by the footwall, there should be a more distinct jump in maximum synkinematic temperatures between hanging wall and footwall in the southernmost exposure (location 16 in Figure 2) where the thrust begins to steepen and ramp downward [cf. *Ruppel and Hodges*, 1994, Figure 2], but this is not observed. There is no discernible horizontal gradient in metamorphic grade within the hanging wall above and to the south of this steeper ramp in the Woodroffe Thrust, indicating that the current geometry differs little from that at the time of Petermann Orogeny metamorphism and activity of the Woodroffe Thrust. If the hanging wall was actively overthrusted on a steep ramp defined by the footwall, the following statements should be true: (1) the maximum metamorphic conditions estimated for shearing at the Mount Fraser klippe (location 11 in Figure 2) should be of similar or higher grade to the conditions estimated from the southernmost outcrop of the footwall (location 16 in Figure 2), and (2) there should be a considerable horizontal metamorphic gradient in maximum metamorphic conditions within the hanging wall due to the steeper ramp geometry of the Woodroffe Thrust (~30°) in its southernmost exposures (locations 13–16 in Figure 5). Neither of the above statements is supported by our geothermobarometric results (Table 1). However, the apparent contradictions can be explained if we consider a model where the footwall is underthrusted below the hanging wall [e.g., *Stewart*, 1997, Figure 17; *Lambeck and Burgess*, 1992, Figure 10a] (Figure 16) rather than the other way around [e.g., *Camacho and McDougall*, 2000; *Edgoose et al*., 2004; *Flottmann et al*., 2004; *Raimondo et al*., 2009]. The overall thrust geometry is not different from previously proposed tectonic models involving either a strike-slip-related, crustal-scale flower-type structure [*Camacho and McDougall*, 2000] or channel flow [*Raimondo et al*., 2009], but only the kinematics of the locations in the hanging wall or footwall relative to the thrust ramp-flat geometry [*Lovering*, 1932]. Rocks brought into immediate contact along the Woodroffe Thrust record effectively the same pressure-temperature conditions. If thermal equilibration was incomplete (as inferred above), this suggests that locations in the hanging wall were not transported from depth along the steepened ramp in the south. This conclusion is in agreement with our observation that the type-A microstructure is never found in the northern locations (1–13 in Figure 2), indicating that the Kelly Hills and Mount Fraser klippen were never at lower crustal level, below the southernmost outcrops of the footwall (locations 14–17 in Figure 2), during the Petermann Orogeny. Such a model is in agreement with the inferred north-side-down offset in the Moho [*Lambeck and Burgess*, 1992; *Aitken et al*., 2009a] occurring across a south dipping thrust plane, e.g., the Woodroffe Thrust rather than the Mann Fault, as the latter records a north-side-up sense of shear [*Camacho and McDougall*, 2000] (Figure 16).

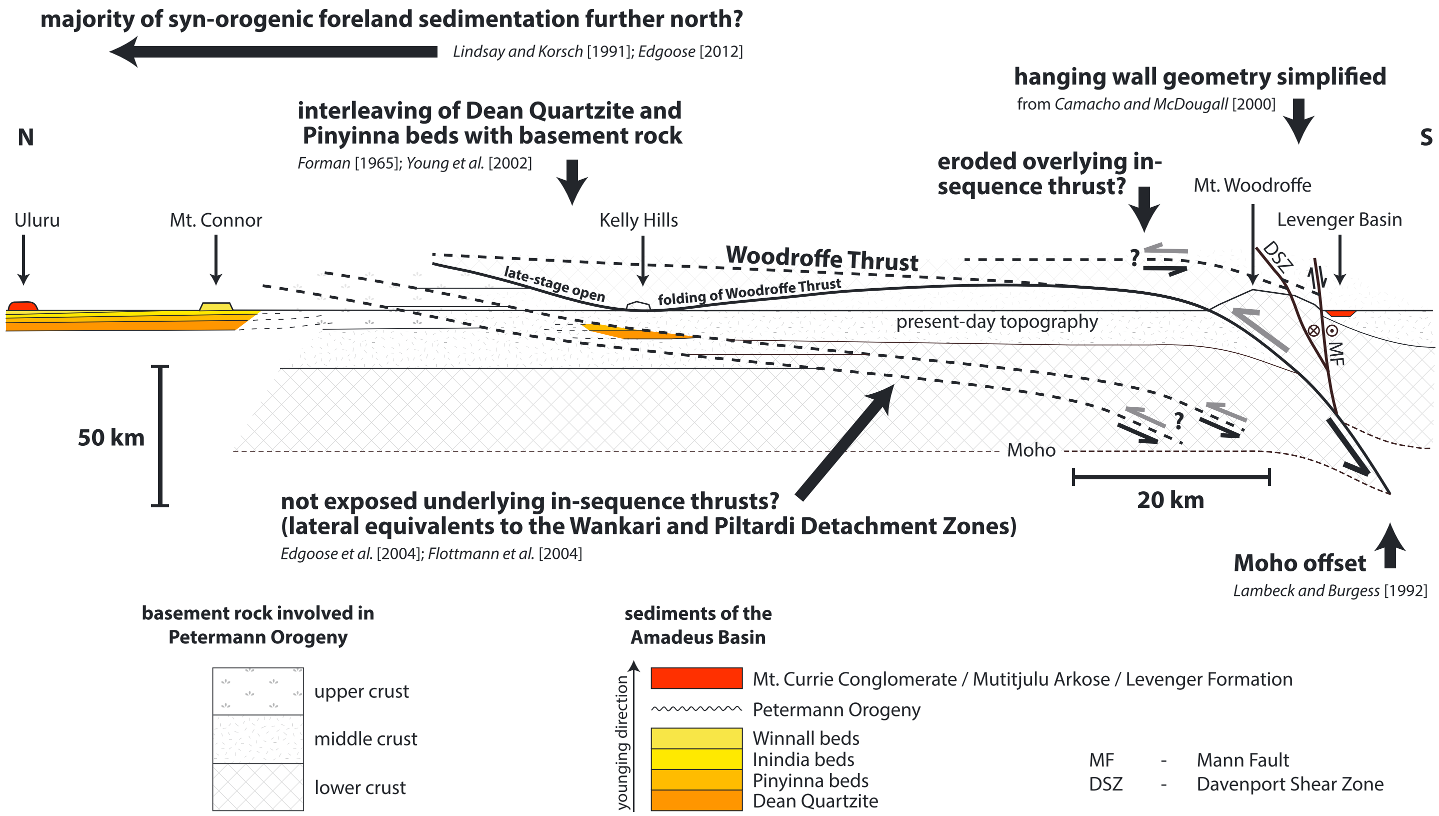

Figure 16. Projected schematic cross section through the central Musgrave Block. The presented profile considers a model of in-sequence underthrusting. The vertical scale is compressed by a factor of 3.5 with respect to the horizontal scale.

The syndeformational geometry of the Woodroffe Thrust, which was largely flat lying and only steepened toward its southernmost exposures, is still preserved in its present-day geometry, despite the large-scale undulations (Figure 5). These undulations could be original [*Raimondo et al.*, 2010] or the result of exhumation but seem to be at least partly due to WNW-ESE shortening, as recorded in the development of steep fold axial planes (Figure 6) and isolated shear zones mainly observed in the hanging wall klippe of Mount Fraser (Figure 7). The documented folding postdates mylonitization and thus the N-S shortening, but the observed emplacement of pseudotachylyte (also involved in high-grade shearing) parallel to the steep fold axial planes (Figure 6) argues for the folding to occur at the same ambient conditions as the ductile shearing along the Woodroffe Thrust. A similar conclusion can be drawn for the two distinct sets of isolated shear zones, associated with approximately N-S and WNW-ESE directed shortening, respectively (Figure 7). Both sets record similar synkinematic metamorphic conditions of circa 550°C and 0.9 GPa, identical to those of the Woodroffe Thrust mylonites at similar latitude (Table 1 and Figure 14). We conclude that the mylonite zone along the Woodroffe Thrust developed during dominant N-S shortening, but that this was complemented by a late-stage WNW-ESE directed shortening. The Kelly Hills and Mount Fraser klippen can thus be interpreted as the result of large-scale fold interference, producing a “dome-and-basin pattern” (Figure 5). Such a late-stage open folding has allowed the klippen to be preserved, since they should be eroded if the Woodroffe Thrust was a purely south dipping planar structure (Figure 16). There is no evidence of significant normal faulting between the preserved klippen in the north and the main exposure of the Woodroffe Thrust farther south, which could otherwise explain the preservation of the Kelly Hills and Mount Fraser klippen. However, steep normal faults most likely do occur locally, with a probable east to ESE strike, as implied from the local downthrow of the Woodroffe Thrust in the Kelly Hills area and from the lack of exposure of Woodroffe Thrust mylonites and associated pseudotachylytes between almost adjacent outcrops of hanging wall and footwall in location 11, east of Mount Fraser (Figure 2).

7.4. Exhumation

It is generally accepted that shearing during the Petermann Orogeny was associated with coeval exhumation to shallower crustal levels [*Camacho et al.*, 1997; *Camacho and McDougall*, 2000; *Flottmann et al.*, 2004]. There is no significant normal faulting in the study area, arguing that exhumation was largely controlled by erosion as a consequence of crustal thickening during the Petermann Orogeny. The associated shortening was accommodated by (1) N-S thrusting along the Woodroffe Thrust, (2) north-side-up and dextral strike-slip movement along the Mann Fault, and (3) strike-slip motion along the Davenport Shear Zone [*Camacho and McDougall*, 2000] (Figure 16).

With the exception of the more northerly dolerite dykes with a retrograde greenschist facies overprint and the extremely rare presence of chlorite, the Woodroffe Thrust mylonites and associated shear zones preserve high-grade mineral assemblages without a late pervasive low-grade metamorphic and structural overprint or brittle faulting. Late generations of pristine pseudotachylytes are locally overgrown by fine-grained garnet, with a mineral chemistry similar to garnet from the dynamically recrystallized mylonites (supporting information F). This is indicative of a syntectonic origin at midcrustal to lower crustal depths, rather than being exhumation related, as proposed by *Lin et al*. [2005]. Our observations and results indicate that the Woodroffe Thrust preserves a midcrustal to lower crustal shearing history and that the observed microstructures were frozen in at midcrustal conditions with no discernible subsequent overprint. The gradual exhumation from lower crustal to midcrustal conditions is preserved in the thrust's southernmost exposures and is reflected structurally in the transition from mylonitic type-A to type-B microstructure (Figure 15) and petrologically in the shift from Grt 1b to Grt 2 (Figure 10). The trend toward lower metamorphic grade indicates that, despite burial of the footwall, the entire Musgrave Block was partially exhumed to shallower crustal depths during the Petermann Orogeny. Exhumation must have occurred syntectonically over the entire Musgrave Block, as $^{40}Ar/^{39}Ar$ cooling ages for biotite and muscovite yield constant values of ~550 Ma over the entire area [*Maboko et al*., 1992; *Camacho and Fanning*, 1995]. However, the general lack of low-grade, exhumation-related features indicates that subsequent exhumation must have occurred in response to further crustal thickening along a different structure. We propose that the Woodroffe Thrust was part of an in-sequence thrust system, with further shortening and crustal thickening (driving erosion and exhumation), accommodated along progressively younger underlying thrust planes farther north in the foreland (Figure 16). This is supported by the fact that the rare occurrences of greenschist facies mineral assemblages are restricted to the northernmost studied outcrops and typically found in the footwall rather than the hanging wall. In-sequence thrusting would additionally account for the virtually unmetamorphosed Neoproterozoic sediments at Mount Conner (Inindia and Winnall beds [*Wells et al*., 1970; *Young et al*., 2002]). Mount Conner is less than 40 km to the north of the northernmost outcrops of the Woodroffe Thrust at Kelly Hills (Figure 16). Assuming that the low-angle geometry of the thrust did not die out immediately north of its last exposure, these units would have been in its footwall and, similar to the Dean Quartzite [*Wells et al*., 1970], should have been metamorphosed under midcrustal conditions. This apparent contradiction is resolved if the Woodroffe Thrust and Mount Conner were originally farther apart during the Petermann Orogeny and only brought closer together by subsequent shortening related to in-sequence thrusting (Figure 16). Such potential thrusts are well exposed farther west in the Petermann nappe complex (Wankari and Piltardi Detachment Zones [*Scrimgeour et al*., 1999; *Edgoose et al*., 2004; *Flottmann et al*., 2004]), but there is no exposure of this in the frontal region of our study area. Nevertheless, similar interleaving of Precambrian basement rock with the basal sedimentary units of the Amadeus Basin (Dean Quartzite and Pinyinna beds [*Wells et al*., 1970] (Figure 16) has been reported [*Forman*, 1965] and is apparent just west of Kelly Hills [*Young et al*., 2002] (Figure 2). In-sequence thrusting is contrary to the synthetic structural evolution proposed by *Scrimgeour et al*. [1999], who consider an out-of-sequence model with, from oldest to youngest, (1) thin-skinned deformation, (2) nappe development along the Wankari and Piltardi Detachment Zones, and (3) late thrusting along the Woodroffe Thrust.

7.5. Crustal Thickness

A model of continuous in-sequence underthrusting during the Petermann, and possibly also during the subsequent Alice Springs Orogeny, provides a potential explanation for why the Musgrave Block still preserves a present-day crustal thickness of ~50 km [*Aitken et al*., 2009a], which should have been nearly 80 km at the time of thrusting, considering that the now exhumed parts were formerly at midcrustal to lower crustal level. An 80 km thick crust, unless it is extremely dry, should almost certainly show significant melting. This contradiction is resolved if we consider that the present-day crustal thickness of 50 km is the result of further footwall nappes, which were subsequently underthrusted after movement on the Woodroffe Thrust had terminated (Figure 16). An increase in crustal thickness by such nappe stacking would have occurred at a time during which crustal thickness had already been, or was still in the process of being, thinned as a consequence of syndeformational and postdeformational erosional exhumation of the Musgrave Block. The total crustal thickness was thus never 80 km.

7.6. Burial of the Fregon Subdomain

The model presented here focuses on the shearing history of the Woodroffe Thrust and its exhumation during the Petermann Orogeny. We have not attempted to constrain the crustal evolution and configuration of the central Musgrave Block prior to the onset of the circa 560–520 Ma Petermann Orogeny. *Camacho* [1997] estimated metamorphic conditions in the Fregon Subdomain farther west in the Amata area (western edge of Figure 2) of 750–800°C and 0.7–0.9 GPa during the ~1200 Ma Musgravian Orogeny, and thus lower values than previous estimates of 820–900°C and 1.1–1.4 GPa by *Maboko et al.* [1989, 1991] and 850–900°C and ~1.2 GPa by *Ellis and Maboko* [1992]. *Maboko et al.* [1989, 1991] and *Ellis and Maboko* [1992] argued that these lower crustal granulite facies rocks subsequently cooled isobarically into the eclogite facies. However, based on the presence of magmatic olivine in the Alcurra Dolerite and the absence of magmatic garnet in the Amata Dolerite, *Camacho* [1997] concluded that these dykes must have crystallized at pressures $<$0.5–0.6 GPa. It follows that the host granulites in the Amata-Ernabella area of the Fregon Subdomain (Figure 2) should have been exhumed to midcrustal or upper crustal levels prior to the onset of the Petermann Orogeny. The predominance of Musgrave Block-derived zircon ages in basal units of the southern Amadeus Basin also indicates at least partial exposure of the Musgrave Block from around 1040 Ma [*Camacho et al*., 2015]. This raises the question of how the Fregon Subdomain was subsequently buried to depths corresponding to ~1.2 GPa during the Petermann Orogeny [*Camacho et al*., 1997]. The proposed model of in-sequence underthrusting potentially provides an explanation, if we consider the former existence of a now entirely eroded thrust plane structurally located above the Fregon Subdomain (Figure 16). The footwall of this hypothetical fault (Fregon Subdomain) would have been buried by underthrusting until the accommodation of shortening shifted to a younger, underlying in-sequence thrust plane (Woodroffe Thrust). The backstop to crustal shortening during the Petermann Orogeny appears to have been the Mann Fault, as it is the only structure in the study area that records a significant jump in metamorphism, with high-pressure assemblages restricted to its northern side. Even though the westward continuation of the Mann Fault is unclear, this metamorphic jump is evident from the regional distribution of garnet-bearing versus non-garnet-bearing dolerite dykes [*Glikson et al*., 1996, Figure 140], as well as the occurrence of unmetamorphosed circa 1030–1070 Ma Tollu Group volcanics in the western Musgrave Block south of the extrapolated continuation of the Mann Fault [*Glikson et al*., 1996, Figure 97].

7.7. Synorogenic Sedimentary Rocks

Synorogenic sedimentary rocks associated with erosion during the Petermann Orogeny are only found in the western foreland of the Musgrave Block (Mount Currie Conglomerate and Mutitjulu Arkose [*Forman*, 1966; *Wells et al*., 1970; *Young et al*., 2002]) (Figure 16) and possibly in hinterland pull-apart basins (Levenger and Moorilyanna Formation) [*Major and Conor*, 1993; *Aitken et al*., 2009b] (Figures 2 and 16). The affinity of the Mount Currie Conglomerate and Mutitjulu Arkose with the Petermann Orogeny has recently been challenged [*Haines et al*., 2016]. Nevertheless, syntectonic foreland deposits, if present, are generally too narrow and not voluminous enough to have formed by erosion of a large-scale nappe structure during a major tectonic event, such as the Petermann Orogeny [*Wells et al*., 1970; *Shaw et al*., 1991]. This problem was previously recognized by *Flottmann et al*. [2004] in the inferred western extension of the Woodroffe Thrust, who argued that a weak lithosphere produced narrow but deep foreland basins, which overfilled, resulting in the transport of synorogenic sediments northward for several hundred kilometers to depocenters in and beyond the northern Amadeus Basin [*Lindsay and Korsch*, 1991]. However, this explanation becomes less appealing in the central and eastern Musgrave Block, where the thrust developed in strong basement rocks with an inferred low geothermal gradient (~16°C/km). Similarly, the movement of depositional loci has been proposed as a consequence of platform development in the southern part of the Amadeus Basin during the Petermann Orogeny, restricting sedimentation in the immediate foreland [*Edgoose*, 2012].

7.8. Woodroffe Thrust Precursor

Our results show that, throughout the current study area, the Woodroffe Thrust was nearly flat lying during the Petermann Orogeny. Localization of ductile deformation along an almost flat-lying surface would require the thrust zone to be extremely weak [*Hubbert and Rubey*, 1959]. However, large volumes of pretectonic and syntectonic pseudotachylyte [*Bell*, 1978; *Camacho et al*., 1995] and the presence of fractured garnet (Figure 10) argue for a strong behavior [*Trepmann and Stöckhert*, 2002; *Sibson and Toy*, 2006], at least transiently. Unless the Woodroffe Thrust initiated with a steeper dip and was pretectonically or syntectonically rotated into a flat-lying orientation (for which there is no evidence), the highly misoriented, low-angle geometry requires a weaker precursor structure for the Woodroffe Thrust. This precursor was potentially a single planar structure, since the Woodroffe Thrust is continuous over several hundred kilometers along strike, without any evidence for amalgamation of smaller shear zones into this major structure. In particular, Petermann Orogeny shear zones in the well-exposed hanging wall in the southern part of the study area are predominantly strike slip (e.g., North Davenport and Davenport Shear Zones [*Collerson et al*., 1972; *Camacho et al*., 1997]) and there are no known important top-to-north thrusts that could represent imbricates of the Woodroffe Thrust. Under amphibolite facies conditions, brittle features, such as fractures and veins [e.g., *Segall and Simpson*, 1986; *Mancktelow and Pennacchioni*, 2005; *Fusseis et al*., 2006; *Pennacchioni and Mancktelow*, 2007] or pseudotachylytes [e.g., *Pennacchioni and Cesare*, 1997; *Pittarello et al*., 2012], lithological discontinuities, such as dykes [e.g., *Christiansen and Pollard*, 1997; *Mancktelow and Pennacchioni*, 2005; *Pennacchioni and Mancktelow*, 2007; *Pennacchioni and Zucchi*, 2013], or inherited crustal-scale suture zones [e.g., *Busch et al*., 1997; *Tikoff et al*., 2001] can act as planar rheological boundaries and nucleation sites for shear deformation. The different possibilities are discussed below.

Myers et al. [1996] proposed a proto-Woodroffe Thrust, representing an inherited suture between the north, south, and west Australian cratons (Figure 1). Despite the general lack of evidence for such a structure, the reactivation of preexisting Mesoproterozoic shear zones controlling the architecture during the Petermann Orogeny has repeatedly been invoked [*Hand and Sandiford*, 1999; *Aitken and Betts*, 2009a, 2009b]. The supporting evidence is limited to the observation that faults related to the Petermann Orogeny are parallel to Mesoproterozoic fabrics in the Musgrave Block [*Hand and Sandiford*, 1999]. However, this argument does not hold in the study area, as the Musgravian fabrics trend approximately N-S to SW-NE, while Petermann fabrics are oriented E-W. Furthermore, based on strong similarities in structural and magmatic history in the hanging wall and footwall of the Woodroffe Thrust prior to thrusting, *Camacho and Fanning* [1995] and *Scrimgeour et al*. [1999] suggested that the juxtaposed units represent different crustal levels of the same terrane, rather than different geological terranes or cratons. This argues against an inherited suture as a possible precursor.

Although not fully understood, *Camacho et al*. [1997] reported an apparent spatial association between dolerite dykes and shear zones in the Davenport Shear Zone. This relationship may be applicable on outcrop scale, but not on a regional scale, as neither the Alcurra nor the Amata Dolerite swarm is concordant with or overprinted by the Woodroffe Thrust along its entire length [*Camacho et al*., 1991; *Zhao et al*., 1994]. Indeed, it is clear from satellite imagery that the Woodroffe Thrust discordantly crosscuts (commonly at low angles) multitudes of such dolerite dykes in the immediate hanging wall, without any tendency to merge into them. This is not what would be expected if the Woodroffe Thrust mylonites were viscous in rheology and the dolerite dykes were relatively weak, i.e., had a lower effective viscosity [*Grujic and Mancktelow*, 1998; *Mancktelow*, 2002].

A common feature reported from all major exposures along strike of the Woodroffe Thrust is the several tens to hundreds of meters wide zone of pseudotachylyte in the immediate hanging wall, as recognized in all well-exposed outcrops of the Woodroffe Thrust in the central Musgrave Block [*Collerson et al*., 1972; *Bell*, 1978; *Camacho et al*., 1995; *Lin et al*., 2005]. Farther west, in the Petermann Ranges, the fault is not exposed [*Scrimgeour et al*., 1999] and can only be inferred from aeromagnetic and regional gravity data [*Forman and Shaw*, 1973; *Pharaoh*, 1990]. The westernmost exposures are only very small, sparse, and isolated [*Stewart*, 1995, 1997]. *Stewart* [1995, 1997] does not mention the occurrence of pseudotachylyte in these outcrops, but several kilometers south, farther into the hanging wall, *Glikson and Mernagh* [1990] report large volumes of pseudotachylyte. Nevertheless, the Woodroffe Thrust is certainly best exposed in the central Musgrave Block, where the current study and the works by *Collerson et al*. [1972], *Bell* [1978], and *Camacho et al*. [1995] were conducted. Pseudotachylytes preserved inside the mylonitic zone of the Woodroffe Thrust were inferred to be of syntectonic or posttectonic origin [*Bell*, 1978; *Camacho et al*., 1995]. However, the vast majority of pseudotachylytes is located in the immediate, largely unsheared hanging wall. These pseudotachylytes most likely formed prior to the ductile shearing history along the Woodroffe Thrust, as they are marginally reworked into the mylonites. Pseudotachylytes have been identified as preferential nucleation sites for shear deformation [*Passchier*, 1982; *Pennacchioni and Cesare*, 1997; *Lund and Austrheim*, 2003; *Austrheim and Andersen*, 2004; *Andersen and Austrheim*, 2006; *Pittarello et al*., 2012; *Hawemann et al*., 2014; *Menegon et al*., 2014; *Wex et al*., 2014]. This is supported by the spatial association between shear zones and pseudotachylytes in the Woodroffe Thrust, as reported by *Camacho et al*. [1995]. We therefore propose that such a pseudotachylyte-rich zone was most likely the necessary precursor for initial localization of the Woodroffe Thrust. This zone is in part still preserved in the nonmylonitized hanging wall, because ductile deformation preferentially localized into the footwall [*Camacho et al*., 1995; *Flottmann et al*., 2004], where it overprinted and obliterated precursor pseudotachylytes during mylonitization.

The Woodroffe Thrust is several hundred kilometers long, suggesting that any potential precursor was at least of similar dimensions. If this precursor was a pseudotachylyte-rich zone, it must have developed on a crustal-scale seismic fault similar to a present-day megathrust and capable of rupturing the center of the Australian continent along a strike length of 600 km or more. The size of the Woodroffe Thrust is comparable with the dimensions of major earthquake ruptures along subduction zones such as, for example, the M_w 9.0 Sumatra-Andaman megathrust earthquake of 2004, which had a rupture length of ~1200 km and maximum thrust displacements of 10–20 m [*Ammon et al*., 2005; *Lomax*, 2005; *Ni et al*., 2005; *Park et al*., 2005; *Stein and Okal*, 2005; *Vigny et al*., 2005; *Lambotte et al*., 2006]. Similarly, the M_w 9.5 great Chilean earthquake of 1960 had a rupture length of ~1000 km and maximum thrust displacements of 20–40 m [*Benioff et al*., 1961; *Press et al*., 1961; *Plafker and Savage*, 1970; *Cifuentes*, 1989]. However, an important difference is that these major earthquakes developed on existing plate boundaries and not within a continental plate. A large earthquake rupturing the interior of the Australian continent is unlikely if considered solely within the paradigm of plate tectonics, with major earthquakes concentrated at plate boundaries, but it could account for the presence of a pseudotachylyte-rich zone continuous over hundreds of kilometers. A single seismic precursor fault is consistent with the lack of any significant set of secondary faults or shear zone structures rooting into the current Woodroffe Thrust. However, the problem of the regional-scale shallow original dip of the thrust remains. This can be related to the preexisting geometry of the precursor but, in the absence of a plate boundary, the problem then becomes how this precursor structure itself had such a low dip. If, as proposed here, the precursor for ductile deformation was a pseudotachylyte-rich zone formed through seismic fracture, then the unsolved problem is how such a large, low-angle, seismic rupture could develop in the very center of a continent.

8. Conclusions

The current study has identified an older annealed and a younger nonannealed microstructure within the Woodroffe Thrust mylonites. These microstructures are interpreted to represent two different stages of the shearing history at lower crustal and midcrustal levels, respectively. The associated ambient metamorphic conditions are estimated to be ~650°C and 1.0–1.3 GPa (annealed lower crustal microstructure) and in the range of circa 520–620°C and 0.8–1.1 GPa (nonannealed midcrustal microstructure). The distribution of the metamorphic assemblages is best explained by underthrusting of the footwall rather than overthrusting of the hanging wall.

In contrast to the generally assumed moderate dip (≥30°) of a thick-skinned shear zone at midcrustal levels, the Woodroffe Thrust was originally flat lying along a ~60 km long N-S transect, with an average dip angle of ≤6° in the direction of tectonic transport. This geometry was only marginally modified by a late-stage component of WNW-ESE shortening, which produced the thrust's present-day undulate geometry.

The microstructures and mineral assemblages within the Woodroffe Thrust were frozen in at dominantly midcrustal conditions, with further shortening and crustal thickening potentially accommodated along progressively younger, underlying, in-sequence thrusts in the foreland. Partial exhumation of the entire region occurred by syntectonic erosion during the Petermann Orogeny.

The thick-skinned Woodroffe Thrust requires a weak precursor structure along which it nucleated, in order to explain its low-angle geometry. This structure was possibly a single horizon that was over 600 km long and characterized by an exceptionally high abundance of pseudotachylyte. If this represents a single seismic rupture event, it would correspond to an earthquake with a potential magnitude of M_w 8–9, developed at midcrustal to lower crustal depths in an intracontinental setting.

Acknowledgments

We thank the communities of the Anangu Pitjantjatjara Yankunytjatjara Lands (APY) for granting us access to the Musgrave Ranges. Logistical support from the Northern Territory Geological Survey (NTGS) of Australia, B. Tikoff (University of Wisconsin, Madison), and Shane and Alethea Nicolle is gratefully recognized. We further acknowledge the support of the Scientific Center for Optical and Electron Microscopy (ScopeM), in particular K. Kunze, at the ETH, Zurich. This project was financed by the Swiss National Science Foundation (SNF) grant 200021_146745. Supplementary data are available in the supporting information "A" to "F" and further information can be obtained on request from the corresponding author.

References

Aitken, A. R. A., and P. G. Betts (2009a), Constraints on the Proterozoic supercontinent cycle from the structural evolution of the south-central Musgrave Province, central Australia, *Precambrian Res.*, *168*(3–4), 284–300, doi:10.1016/j.precamres.2008.10.006.

Aitken, A. R. A., and P. G. Betts (2009b), Multi-scale integrated structural and aeromagnetic analysis to guide tectonic models: An example from the eastern Musgrave Province, Central Australia, *Tectonophysics*, *476*(3–4), 418–435, doi:10.1016/j.tecto.2009.07.007.

Aitken, A. R. A., P. G. Betts, R. F. Weinberg, and D. Gray (2009a), Constrained potential field modeling of the crustal architecture of the Musgrave Province in central Australia: Evidence for lithospheric strengthening due to crust-mantle boundary uplift, *J. Geophys. Res.*, *114*, B12405, doi:10.1029/2008JB006194.

Aitken, A. R. A., P. G. Betts, and L. Ailleres (2009b), The architecture, kinematics, and lithospheric processes of a compressional intraplate orogen occurring under Gondwana assembly: The Petermann Orogeny, central Australia, *Lithosphere*, *1*(6), 343–357, doi:10.1130/L39.1.

Ammon, C. J., et al. (2005), Rupture process of the 2004 Sumatra-Andaman earthquake, *Science*, *308*(5725), 1133–1139, doi:10.1126/science.1112260.

Andersen, T. B., and H. Austrheim (2006), Fossil earthquakes recorded by pseudotachylytes in mantle peridotite from the Alpine subduction complex of Corsica, *Earth Planet. Sci. Lett.*, *242*(1–2), 58–72, doi:10.1016/j.epsl.2005.11.058.

Anderson, E. M. (1905), The dynamics of faulting, *Trans. Edinb. Geol. Soc.*, *8*, 387–402, doi:10.1144/transed.8.3.387.

Anderson, E. M. (1951), *The Dynamics of Faulting and Dyke Formation with Application to Britain*, Oliver & Boyd, Edinburgh.

Austrheim, H., and T. B. Andersen (2004), Pseudotachylytes from Corsica: Fossil earthquakes from a subduction complex, *Terra Nova*, *16*(4), 193–197, doi:10.1111/j.1365-3121.2004.00551.x.

Ballhaus, C., and A. Y. Glikson (1995), The petrology of layered mafic-ultramafic intrusions of the Giles Complex, western Musgrave Block, Western Australia, *AGSO J. Aust. Geol. Geophys.*, *16*(1/2), 69–90.

Bell, T. H. (1978), Progressive deformation and reorientation of fold axes in a ductile mylonite zone: The Woodroffe Thrust, *Tectonophysics*, *44*(1–4), 285–320, doi:10.1016/0040-1951(78)90074-4.

Bell, T. H., and S. E. Johnson (1989), The role of deformation partitioning in the deformation and recrystallization of plagioclase and K-feldspar in the Woodroffe Thrust mylonite zone, central Australia, *J. Metamorph. Geol.*, *7*(2), 151–168, doi:10.1111/j.1525-1314.1989.tb00582.x.

Bell, T. H., and S. E. Johnson (1992), Shear sense: A new approach that resolves conflicts between criteria in metamorphic rocks, *J. Metamorph. Geol.*, *10*(1), 99–124, doi:10.1111/j.1525-1314.1992.tb00074.x.

Benioff, H., F. Press, and S. Smith (1961), Excitation of the free oscillations of the Earth by earthquakes, *J. Geophys. Res.*, *66*(2), 605–619, doi:10.1029/JZ066i002p00605.

Boyd, F. R., and J. L. England (1961), Melting of silicates at high pressures, in *Carnegie Institution of Washington Year Book 60*, pp. 113–125, Port City Press, Baltimore.

Braun, J., and R. Shaw (2001), A thin-plate model of Palaeozoic deformation of the Australian lithosphere: Implications for understanding the dynamics of intracratonic deformation, in *Continental Reactivation and Reworking*, *Spec. Publ.*, vol. 184, edited by J. A. Miller et al., pp. 165–193, Geol. Soc., London.

Brewer, J. A., and D. K. Smythe (1984), MOIST and the continuity of crustal reflector geometry along the Caledonian-Appalachian orogen, *J. Geol. Soc.*, *141*, 105–120, doi:10.1144/gsjgs.141.1.0105.

Brewer, J. A., S. B. Smithson, J. E. Oliver, S. Kaufman, and L. D. Brown (1980), The Laramide Orogeny: Evidence from COCORP deep crustal seismic profiles in the Wind River Mountains, Wyoming, *Tectonophysics*, *62*(3–4), 165–189, doi:10.1016/0040-1951(80)90191-2.

Busch, J. P., K. Mezger, and B. A. van der Pluijm (1997), Suturing and extensional reactivation in the Grenville orogen, Canada, *Geology*, *25*(6), 507–510, doi:10.1130/0091-7613(1997)025<0507:SAERIT>2.3.CO;2.

Byerlee, J. (1978), Friction of rocks, *Pure Appl. Chem.*, *116*(4), 615–626, doi:10.1007/BF00876528.

Camacho, A. (1997), An isotopic study of deep-crustal orogenic processes: Musgrave Block, Central Australia, PhD thesis, The Australian Natl. Univ., Canberra.

Camacho, A., and C. M. Fanning (1995), Some isotopic constraints on the evolution of the granulite and upper amphibolite facies terranes in the eastern Musgrave Block, central Australia, *Precambrian Res.*, *71*(1–4), 155–181, doi:10.1016/0301-9268(94)00060-5.

Camacho, A., and I. McDougall (2000), Intracratonic, strike-slip partitioned transpression and the formation and exhumation of eclogite facies rocks: An example from the Musgrave Block, central Australia, *Tectonics*, *19*(5), 978–996, doi:10.1029/1999TC001151.

Camacho, A., B. Simons, and P. W. Schmidt (1991), Geological and palaeomagnetic significance of the Kulgera dyke swarm, Musgrave Block, NT, Australia, *Geophys. J. Int.*, *107*(1), 37–45, doi:10.1111/j.1365-246X.1991.tb01154.x.

Camacho, A., R. H. Vernon, and J. D. Fitz Gerald (1995), Large volumes of anhydrous pseudotachylyte in the Woodroffe Thrust, eastern Musgrave Ranges, Australia, *J. Struct. Geol.*, *17*(3), 371–383, doi:10.1016/0191-8141(94)00069-C.

Camacho, A., W. Compston, M. McCulloch, and I. McDougall (1997), Timing and exhumation of eclogite facies shear zones, Musgrave Block, central Australia, *J. Metamorph. Geol.*, *15*(6), 735–751, doi:10.1111/j.1525-1314.1997.00053.x.

Camacho, A., I. McDougall, R. Armstrong, and J. Braun (2001), Evidence for shear heating, Musgrave Block, central Australia, *J. Struct. Geol.*, *23*(6–7), 1007–1013, doi:10.1016/S0191-8141(00)00172-3.

Camacho, A., B. J. Hensen, and R. Armstrong (2002), Isotopic test of a thermally driven intraplate orogenic model, Australia, *Geology*, *30*(10), 887–890, doi:10.1130/0091-7613(2002)030<0887:ITOATD>2.0.CO;2.

Camacho, A., P. Yang, and A. Frederiksen (2009), Constraints from diffusion profiles on the duration of high-strain deformation in thickened crust, *Geology*, *37*(8), 755–758, doi:10.1130/G25753A.1.

Camacho, A., R. Armstrong, D. W. Davis, and A. Bekker (2015), Early history of the Amadeus Basin: Implications for the existence and geometry of the Centralian Superbasin, *Precambrian Res.*, *259*, 232–242, doi:10.1016/j.precamres.2014.12.004.

Cho, W. J., S. Kwon, and J. W. Choi (2009), The thermal conductivity for granite with various water contents, *Eng. Geol.*, *107*(3–4), 167–171, doi:10.1016/j.enggeo.2009.05.012.

Christiansen, P. P., and D. D. Pollard (1997), Nucleation, growth and structural development of mylonitic shear zones in granitic rock, *J. Struct. Geol.*, *19*(9), 1159–1172, doi:10.1016/S0191-8141(97)00025-4.

Cifuentes, I. L. (1989), The 1960 Chilean earthquakes, *J. Geophys. Res.*, *94*(B1), 665–680, doi:10.1029/JB094iB01p00665.

Claeson, D. T. (1998), Coronas, reaction rims, symplectites and emplacement depth of the Rymmen gabbro, Transscandinavian Igneous Belt, southern Sweden, *Mineral. Mag.*, *62*(6), 743–757, doi:10.1180/002646198548133.

Clarke, G. L. (1992), *Record 1992/33: Field Relationships and Tectonic History of the Hinckley Gabbro Felsic to Mafic Granulites and Granitoids, West Hinckley Range and Champ de Mars Areas, Tomkinson Ranges, Musgrave Block, WA*, Bur. of Miner. Resour., Geol. and Geophys., Canberra.

Clarke, G. L., I. S. Buick, A. Y. Glikson, and A. J. Stewart (1995), Structural and pressure-temperature evolution of host rocks of the Giles Complex, western Musgrave Block, central Australia: Evidence for multiple high-pressure events, *AGSO J. Aust. Geol. Geophys.*, *16*(1/2), 127–146.

Collerson, K. D., R. L. Oliver, and R. W. R. Rutland (1972), An example of structural and metamorphic relationships in the Musgrave orogenic belt, central Australia, *J. Geol. Soc. Aust.*, *18*(4), 379–393, doi:10.1080/00167617208728776.

Cooper, F. J., J. P. Platt, R. Anczkiewicz, and M. J. Whitehouse (2010), Footwall dip of a core complex detachment fault: Thermobarometric constraints from the northern Snake Range (Basin and Range, USA), *J. Metamorph. Geol.*, *28*(9), 997–1020, doi:10.1111/j.1525-1314.2010.00907.x.

Coward, M. P. (1983), Thrust tectonics, thin skinned or thick skinned, and the continuation of thrusts to deep in the crust, *J. Struct. Geol.*, *5*(2), 113–123, doi:10.1016/0191-8141(83)90037-8.

Davis, D., J. Suppe, and F. A. Dahlen (1983), Mechanics of fold-and-thrust belts and accretionary wedges, *J. Geophys. Res.*, *88*(B2), 1153–1172, doi:10.1029/JB088iB02p01153.

Donath, F. A. (1961), Experimental study of shear failure in anisotropic rocks, *Geol. Soc. Am. Bull.*, *72*(6), 985–989, doi:10.1130/0016-7606(1961)72[985:ESOSFI]2.0.CO;2.

Droop, G. T. R. (1987), A general equation for estimating Fe^{3+} concentrations in ferromagnesian silicates and oxides from microprobe analyses, using stoichiometric criteria, *Mineral. Mag.*, *51*(361), 431–435, doi:10.1180/minmag.1987.051.361.10.

Durocher, K. E., T. K. Kyser, J. Marlatt, and A. Hanly (2003), New $^{40}Ar/^{39}Ar$ ages from the central Paterson Orogen, Western Australia, *Aust. J. Earth Sci.*, *50*(4), 601–610, doi:10.1046/j.1440-0952.2003.01011.x.

Eckert, J. O., R. C. Newton, and O. J. Kleppa (1991), The ΔH of reaction and recalibration of garnet-pyroxene-plagioclase-quartz geobarometers in the CMAS system by solution calorimetry, *Am. Mineral.*, *76*(1), 148–160.

Edgoose, C. J. (2012), The Amadeus Basin, central Australia, *Episodes*, *35*(1), 256–263.

Edgoose, C. J., A. Camacho, G. A. Wakelin-King, and B. A. Simons (1993), *1:250 000 Geological Map Series Explanatory Notes. Kulgera SG 53–5*, 2nd ed., North. Territ. Geol. Surv., Darwin.

Edgoose, C. J., I. R. Scrimgeour, and D. F. Close (2004), *Report 15: Geology of the Musgrave Block, Northern Territory*, North. Territ. Geol. Surv., Darwin.

Ellis, D. J., and M. A. H. Maboko (1992), Precambrian tectonics and the physicochemical evolution of the continental crust. I. The gabbro-eclogite transition revisited, *Precambrian Res.*, *55*(1–4), 491–506, doi:10.1016/0301-9268(92)90041-L.

England, P. C., and A. B. Thompson (1984), Pressure-temperature-time paths of regional metamorphism I. Heat transfer during the evolution of regions of thickened continental crust, *J. Petrol.*, *25*(4), 894–928, doi:10.1093/petrology/25.4.894.

Evins, P. M., R. H. Smithies, H. M. Howard, C. L. Kirkland, M. T. D. Wingate, and S. Bodorkos (2010), *Record 2010/6: Redefining the Giles Event Within the Setting of the 1120–1020 Ma Ngaanyatjarra Rift, West Musgrave Province, Central Australia*, Geol. Surv. of Western Australia, Perth.

Flottmann, T., M. Hand, D. Close, C. Edgoose, and I. Scrimgeour (2004), Thrust tectonic styles of the Intracratonic Alice Springs and Petermann Orogenies, Central Australia, in *AAPG Memoir 82: Thrust Tectonics and Hydrocarbon Systems*, edited by K. R. McClay, pp. 538–557, Tulsa.

Forman, D. J. (1965), *1:250,000 Geological Series Explanatory Notes. Ayers Rock, N.T. SG/52–8*, 1st ed., Bur. of Miner. Resour., Geol. and Geophys., Canberra.

Forman, D. J. (1966), *Report 87: The Geology of the South-Western Margin of the Amadeus Basin, Central Australia*, Bur. of Miner. Resour., Geol. and Geophys., Canberra.

Forman, D. J., and R. D. Shaw (1973), *Bulletin 144: Deformation of the Crust and Mantle in Central Australia*, Bur. of Miner. Resour., Geol. and Geophys., Canberra.

Fossen, H. (2016), *Structural Geology*, 2nd ed., Cambridge Univ. Press, Cambridge.

Fusseis, F., M. R. Handy, and C. Schrank (2006), Networking of shear zones at the brittle-to-viscous transition (Cap de Creus, NE Spain), *J. Struct. Geol.*, *28*(7), 1228–1243, doi:10.1016/j.jsg.2006.03.022.

Fyfe, W. S., N. J. Price, and A. B. Thompson (1978), *Fluids in the Earth's Crust: Their Significance in Metamorphic, Tectonic, and Chemical Transport Processes*, Elsevier, Amsterdam.

Gapais, D. (1989), Shear structures within deformed granites: Mechanical and thermal indicators, *Geology*, *17*(12), 1144–1147, doi:10.1130/0091-7613(1989)017<1144:SSWDGM>2.3.CO;2.

Gardner, P. M., and B. Robins (1974), The olivine-plagioclase reaction: Geological evidence from the Seiland Petrographic Province, northern Norway, *Contrib. Mineral. Petrol.*, *44*(2), 149–156, doi:10.1007/BF00385787.

Glikson, A. Y., and T. P. Mernagh (1990), Significance of pseudotachylite vein systems, Giles basic/ultrabasic complex, Tomkinson Ranges, western Musgrave Block, central Australia, *J. Aust. Geol. Geophys.*, *11*, 509–519.

Glikson, A. Y., A. J. Stewart, C. G. Ballhaus, G. L. Clarke, E. H. J. Feeken, J. H. Leven, J. W. Sheraton, and S. Sun (1996), *Bulletin 239: Geology of the western Musgrave Block, central Australia, with particular reference to the mafic-ultramafic Giles Complex*, edited by M. Curtis and J. Sheraton, Aust. Geol. Surv. Organ., Canberra.

Gordon, S. M., P. Luffi, B. Hacker, J. Valley, M. Spicuzza, R. Kozdon, P. Kelemen, L. Ratshbacher, and V. Minaev (2012), The thermal structure of continental crust in active orogens: Insight from Miocene eclogite and granulite xenoliths of the Pamir Mountains, *J. Metamorph. Geol.*, *30*(4), 413–434, doi:10.1111/j.1525-1314.2012.00973.x.

Gray, C. M. (1977), The geochemistry of central Australian granulites in relation to the chemical and isotopic effects of granulite facies metamorphism, *Contrib. Mineral. Petrol.*, *65*(1), 79–89, doi:10.1007/BF00373573.

Gray, C. M. (1978), Geochronology of granulite-facies gneisses in the western Musgrave Block, central Australia, *J. Geol. Soc. Aust.*, *25*(7), 403–414, doi:10.1080/00167617808729050.

Gray, C. M., and W. Compston (1978), A rubidium-strontium chronology of the metamorphism and prehistory of central Australian granulites, *Geochim. Cosmochim. Acta*, *42*(11), 1735–1747, doi:10.1016/0016-7037(78)90259-4.

Grujic, D., and N. S. Mancktelow (1998), Melt-bearing shear zones: Analogue experiments and comparison with examples from southern Madagascar, *J. Struct. Geol.*, *20*(6), 673–680, doi:10.1016/S0191-8141(98)00006-6.

Haines, P. W., C. L. Kirkland, M. T. D. Wingate, H. Allen, E. A. Belousova, and Y. Gréau (2016), Tracking sediment dispersal during orogenesis: A zircon age and Hf isotope study from the western Amadeus Basin, Australia, *Gondwana Res.*, *37*, 324–347, doi:10.1016/j.gr.2015.08.011.

Hand, M., and M. Sandiford (1999), Intraplate deformation in central Australia, the link between subsidence and fault reactivation, *Tectonophysics*, *305*(1–3), 121–140, doi:10.1016/S0040-1951(99)00009-8.

Handin, J. (1969), On the Coulomb-Mohr failure criterion, *J. Geophys. Res.*, *74*(22), 5343–5348, doi:10.1029/JB074i022p05343.

Hariya, Y., and G. C. Kennedy (1968), Equilibrium study of anorthite under high pressure and high temperature, *Am. J. Sci.*, *266*(3), 193–203, doi:10.2475/ajs.266.3.193.

Hawemann, F., N. Mancktelow, S. Wex, A. Camacho, and G. Pennacchioni (2014), Strain localization on different scales and the importance of brittle precursors during deformation in the lower crust (Davenport Shear Zone, Central Australia), *Geophys. Res. Abstr.*, *16*, 5009.

Healy, D., R. H. Sibson, Z. Shipton, and R. Butler (2012), Stress, faulting, fracturing and seismicity: The legacy of Ernest Masson Anderson, in *Faulting, Fracturing and Igneous Intrusion in the Earth's Crust*, *Spec. Publ.*, vol. 367, edited by D. Healy et al., pp. 1–6, Geol. Soc., London.

Holdaway, M. J. (1971), Stability of andalusite and the aluminum silicate phase diagram, *Am. Mineral.*, *271*(2), 97–131, doi:10.2475/ajs.271.2.97.

Holdaway, M. J. (2000), Application of new experimental and garnet Margules data to the garnet-biotite geothermometer, *Am. Mineral.*, *85*(7–8), 881–892, doi:10.2138/am-2000-0701.

Holdaway, M. J. (2001), Recalibration of the GASP geobarometer in light of recent garnet and plagioclase activity models and versions of the garnet-biotite geothermometer, *Am. Mineral.*, *86*(10), 1117–1129, doi:10.2138/am-2001-1001.

Hubbert, M. K., and W. W. Rubey (1959), Role of fluid pressure in mechanics of overthrust faulting I. Mechanics of fluid-filled porous solids and its application to overthrust faulting, *Bull. Geol. Soc. Am.*, *70*(2), 115–166, doi:10.1130/0016-7606(1959)70[115:ROFPIM]2.0.CO;2.

Jäger, J. C., and N. G. W. Cook (1979), *Fundamentals of Rock Mechanics*, 3rd ed., Chapman & Hall, London.

Kretz, R., P. Jones, and R. Hartree (1989), Grenville metagabbro complexes of the Otter Lake area, Quebec, *Can. J. Earth Sci.*, *26*(2), 215–230, doi:10.1139/e89-018.

Krogh Ravna, E. (2000), The garnet-clinopyroxene Fe^{2+}- Mg geothermometer: An updated calibration, *J. Metamorph. Geol.*, *18*(2), 211–219, doi:10.1046/j.1525-1314.2000.00247.x.

Lambeck, K., and G. Burgess (1992), Deep crustal structure of the Musgrave Block, central Australia: Results from teleseismic travel-time anomalies, *Aust. J. Earth Sci.*, *39*, 1–19, doi:10.1080/08120099208727996.

Lambotte, S., L. Rivera, and J. Hinderer (2006), Rupture length and duration of the 2004 Aceh-Sumatra earthquake from the phases of the Earth's gravest free oscillations, *Geophys. Res. Lett.*, *33*, L03307, doi:10.1029/2005GL024090.

Lin, A., T. Maruyama, S. Aaron, K. Michibayashi, A. Camacho, and K. Kano (2005), Propagation of seismic slip from brittle to ductile crust: Evidence from pseudotachylyte of the Woodroffe Thrust, central Australia, *Tectonophysics*, *402*(1–4), 21–35, doi:10.1016/j.tecto.2004.10.016.

Lindsay, J. F., and R. J. Korsch (1991), The evolution of the Amadeus Basin, central Australia, in *Geological and Geophysical Studies in the Amadeus Basin, Central Australia*, edited by R. J. Korsch and J. M. Kennar, pp. 7–32, Bur. of Miner. Resour., Geol. and Geophys., Canberra.

Lomax, A. (2005), Rapid estimation of rupture extent for large earthquakes: Application to the 2004, M9 Sumatra-Andaman mega-thrust, *Geophys. Res. Lett.*, *32*, L10314, doi:10.1029/2005GL022437.

Lovering, T. S. (1932), Field evidence to distinguish over-thrusting from underthrusting, *J. Geol.*, *40*(7), 651–663.

Lund, M. G., and H. Austrheim (2003), High-pressure metamorphism and deep-crustal seismicity: Evidence from contemporaneous formation of pseudotachylytes and eclogite facies coronas, *Tectonophysics*, *372*(1–2), 59–83, doi:10.1016/S0040-1951(03)00232-4.

Maboko, M. A. H., I. McDougall, and P. K. Zeitler (1989), Metamorphic P-T path of granulites in the Musgrave Ranges, central Australia, in *Evolution of Metamorphic Belts*, edited by J. S. Daly, R. A. Cliff, and B. W. D. Yardley, *Geol. Soc. London Spec. Publ.*, 43, pp. 303–307.

Maboko, M. A. H., I. S. Williams, and W. Compston (1991), Zircon U-Pb chronometry of the pressure and temperature history of granulites in the Musgrave Ranges, Central Australia, *J. Geol.*, *99*(5), 675–697.

Maboko, M. A. H., I. McDougall, P. K. Zeitler, and I. S. Williams (1992), Geochronological evidence for ~ 530–550 Ma juxtaposition of two Proterozoic metamorphic terranes in the Musgrave Ranges, central Australia, *Aust. J. Earth Sci.*, *39*(4), 457–471, doi:10.1080/08120099208728038.

Major, R. B. (1970), Woodroffe Thrust zone in the Musgrave Ranges, *Q. Geol. Notes issued by Geol. Surv. South Aust.*, *35*, 9–11.

Major, R. B. (1973), *Explanatory Notes for the Woodroffe 1:250 000 Geological Map SG/52–12*, 1st ed., Geol. Surv. of South Aust., Adelaide.

Major, R. B., and C. H. H. Conor (1993), Musgrave Block, in *Bulletin 54: The Geology of South Australia. Volume 1. The Precambrian*, edited by J. F. Drexel, W. V. Preiss, and A. J. Parker, pp. 156–167, Geol. Surv. of South Aust., Adelaide.

Major, R. B., J. E. Johnson, B. Leeson, R. C. Mirams, and B. P. Thomson (1967), *1:250 000 S.A. Geological Atlas Series Sheet. Woodroffe SG 52–12 Zone 4*, 1st ed., Geol. Surv. of South Aust., Adelaide.

Malavieille, J. (1984), Modélisation expérimentale des chevauchements imbriqués: Application aux chaînes de montagnes, *Bull. la Soc. Géol. Fr.*, *S7–XXVI*(1), 129–138, doi:10.2113/gssgfbull.S7-XXVI.1.129.

Mancktelow, N. S. (2002), Finite-element modelling of shear zone development in viscoelastic materials and its implications for localisation of partial melting, *J. Struct. Geol.*, *24*(6–7), 1045–1053, doi:10.1016/S0191-8141(01)00090-6.

Mancktelow, N. S., and G. Pennacchioni (2005), The control of precursor brittle fracture and fluid-rock interaction on the development of single and paired ductile shear zones, *J. Struct. Geol.*, *27*(4), 645–661, doi:10.1016/j.jsg.2004.12.001.

Maruyama, S., J. G. Liou, and K. Suzuki (1982), The peristerite gap in low-grade metamorphic rocks, *Contrib. Mineral. Petrol.*, *81*(4), 268–276, doi:10.1007/BF00371681.

McLaren, S., M. Sandiford, M. Hand, N. Neumann, L. Wyborn, and I. Bastrakova (2003), The hot southern continent: Heat flow and heat production in Australian Proterozoic terranes, *Geol. Soc. Aust. Spec. Publ.*, *22*, 151–161, doi:10.1130/0-8137-2372-8.157.

Menegon, L., G. Pennacchioni, K. Harris, and E. Wood (2014), High temperature pseudotachylytes and ductile shear zones in dry rocks from the continental lower crust (Lofoten, Norway), *Geophys. Res. Abstr.*, *16*, 12810.

Moore, A. C., and A. D. T. Goode (1978), Petrography and origin of granulite-facies rocks in the western Musgrave Block, Central Australia, *J. Geol. Soc. Aust.*, *25*(5–6), 341–358, doi:10.1080/00167617808729040.

Myers, J. S., R. D. Shaw, and I. M. Tyler (1996), Tectonic evolution of Proterozoic Australia, *Tectonics*, *15*(6), 1431–1446, doi:10.1029/96TC02356.

Newton, R. C., and H. T. Haselton (1981), Thermodynamics of the garnet-plagioclase-Al_2SiO_5-quartz geobarometer, in *Thermodynamics of Minerals and Melts*, edited by R. C. Newton, A. Navrotsky, and B. J. Wood, pp. 131–147, Springer, New York.

Newton, R. C., and D. Perkins (1982), Thermodynamic calibration of geobarometers based on the assemblages garnet-plagioclase-orthopyroxene (clinopyroxene)-quartz, *Am. Mineral.*, *67*(3), 203–222.

Ni, S., H. Kanamori, and D. Helmberger (2005), Energy radiation from the Sumatra earthquake, *Nature*, *434*, 582, doi:10.1038/434582a.

Nishiyama, T. (1983), Steady diffusion model for olivine-plagioclase corona growth, *Geochim. Cosmochim. Acta*, *47*(2), 283–294, doi:10.1016/0016-7037(83)90141-2.

Park, J., K. Anderson, R. Aster, R. Butler, T. Lay, and D. Simpson (2005), Global seismographic network records the great Sumatra-Andaman earthquake, *EOS Trans. Am. Geophys. Union*, *86*(6), 57–64, doi:10.1029/2005EO060001.

Passchier, C. W. (1982), Pseudotachylyte and the development of ultramylonite bands in the Saint-Barthélemy massif, French Pyrenees, *J. Struct. Geol.*, *4*(1), 69–79, doi:10.1016/0191-8141(82)90008-6.

Pennacchioni, G., and B. Cesare (1997), Ductile-brittle transition in pre-Alpine amphibolite facies mylonites during evolution from water-present to water-deficient conditions (Mont Mary nappe, Italian western Alps), *J. Metamorph. Geol.*, *15*(6), 777–791, doi:10.1111/j.1525-1314.1997.00055.x.

Pennacchioni, G., and N. S. Mancktelow (2007), Nucleation and initial growth of a shear zone network within compositionally and structurally heterogeneous granitoids under amphibolite facies conditions, *J. Struct. Geol.*, *29*(11), 1757–1780, doi:10.1016/j.jsg.2007.06.002.

Pennacchioni, G., and E. Zucchi (2013), High temperature fracturing and ductile deformation during cooling of a pluton: The Lake Edison granodiorite (Sierra Nevada batholith, California), *J. Struct. Geol.*, *50*, 54–81, doi:10.1016/j.jsg.2012.06.001.

Perchuk, L. L., and I. V. Lavrent'eva (1983), Experimental investigation of exchange equilibria in the system cordierite-garnet-biotite, in *Kinetics and Equilibrium in Mineral Reactions*, edited by S. K. Saxena, pp. 199–239, Springer, New York.

Pharaoh, T. C. (1990), *Record 1990/5: Aspects of Structural Geology of the Giles Layered Basic/Ultrabasic Complex and Associated Felsic Granulites, Tomkinson Range, Musgrave Block, Central Australia*, Bur. of Min. Resour., Geol. and Geophys., Canberra.

Pittarello, L., G. Pennacchioni, and G. Di Toro (2012), Amphibolite-facies pseudotachylytes in Premosello metagabbro and felsic mylonites (Ivrea Zone, Italy), *Tectonophysics*, *580*, 43–57, doi:10.1016/j.tecto.2012.08.001.

Plafker, G., and J. C. Savage (1970), Mechanism of the Chilean earthquakes of May 21 and 22, 1960, *Geol. Soc. Am. Bull.*, *81*(4), 1001–1030, doi:10.1130/0016-7606(1970)81[1001:MOTCEO]2.0.CO;2.

Platt, J. P. (1986), Dynamics of orogenic wedges and the uplift of high-pressure metamorphic rocks, *Geol. Soc. Am. Bull.*, *97*(9), 1037–1053, doi:10.1130/0016-7606(1986)97<1037:DOOWAT>2.0.CO;2.

Press, F., A. Ben-Menahem, and M. Nafi Toksöz (1961), Experimental determination of earthquake fault length and rupture velocity, *J. Geophys. Res.*, *66*(10), 3471–3485, doi:10.1029/JZ066i010p03471.

Raimondo, T., A. S. Collins, M. Hand, A. Walker-Hallam, R. H. Smithies, P. M. Evins, and H. M. Howard (2009), Ediacaran intracontinental channel flow, *Geology*, *37*(4), 291–294, doi:10.1130/G25452A.1.

Raimondo, T., A. S. Collins, M. Hand, A. Walker-Hallam, R. H. Smithies, P. M. Evins, and H. M. Howard (2010), The anatomy of a deep intracontinental orogen, *Tectonics*, *29*, TC4024, doi:10.1029/2009TC002504.

Raimondo, T., M. Hand, and W. J. Collins (2014), Compressional intracontinental orogens: Ancient and modern perspectives, *Earth Sci. Rev.*, *130*, 128–153, doi:10.1016/j.earscirev.2013.11.009.

Ramsay, J. G., and M. I. Huber (1987), *The Techniques of Modern Structural Geology. Volume 2: Folds and Fractures*, 1st ed., Academic Press, London.

Roberts, E. A., and G. A. Houseman (2001), Geodynamics of central Australia during the intraplate Alice Springs Orogeny: Thin viscous sheet models, in *Continental Reactivation and Reworking*, edited by J. A. Miller et al., *Geol. Soc. London Spec. Publ.*, 184, 139–164, Geological Society, London.

Ruppel, C., and K. V. Hodges (1994), Role of horizontal thermal conduction and finite time thrust emplacement in simulation of pressure-temperature-time paths, *Earth Planet. Sci. Lett.*, *123*(1–3), 49–60, doi:10.1016/0012-821X(94)90256-9.

Sandiford, M., and M. Hand (1998), Controls on the locus of intraplate deformation in central Australia, *Earth Planet. Sci. Lett.*, *162*(1–4), 97–110, doi:10.1016/S0012-821X(98)00159-9.

Sclater, J. G., C. Jaupart, and D. Galson (1980), The heat flow through oceanic and continental crust and the heat loss of the Earth, *Rev. Geophys. Space Phys.*, *18*(1), 269–311, doi:10.1029/RG018i001p00269.

Scrimgeour, I., and D. Close (1999), Regional high-pressure metamorphism during intracratonic deformation: The Petermann Orogeny, central Australia, *J. Metamorph. Geol.*, *17*(5), 557–572, doi:10.1046/j.1525-1314.1999.00217.x.

Scrimgeour, I. R., D. F. Close, and C. J. Edgoose (1999), *1:250,000 Geological Map Series and Explanatory Notes. Petermann Ranges SG52-7*, 2nd ed., North. Territ. Geol. Surv., Darwin.

Segall, P., and C. Simpson (1986), Nucleation of ductile shear zones on dilatant fractures, *Geology*, *14*(1), 56–59, doi:10.1130/0091-7613(1986)14<56:NODSZO>2.0.CO.

Shaw, R. D., M. A. Etheridge, and K. Lambeck (1991), Development of the Late Proterozoic to Mid-Paleozoic, intracratonic Amadeus Basin in central Australia: A key to understanding tectonic forces in plate interiors, *Tectonics*, *10*(4), 688–721, doi:10.1029/90TC02417.

Sibson, R. H. (1990), Rupture nucleation on unfavorably oriented faults, *Bull. Seismol. Soc. Am.*, *80*(6), 1580–1604.

Sibson, R. H. (2012), Reverse fault rupturing: Competition between non-optimal and optimal fault orientations, in *Faulting, Fracturing and Igneous Intrusion in the Earth's Crust*, edited by D. Healy et al., *Geol. Soc. London Spec. Publ.*, 367, 39–50.

Sibson, R. H., and V. G. Toy (2006), The habitat of fault-generated pseudotachylyte: Presence vs. absence of friction-melt, in *Earthquakes: Radiated Energy and the Physics of Faulting*, *Geophys. Monogr. Ser*, vol. 170, edited by R. Abercrombie et al., pp. 153–166, AGU, Washington D. C.

Simpson, C. (1985), Deformation of granitic rocks across the brittle-ductile transition, *J. Struct. Geol.*, *7*(5), 503–511, doi:10.1016/0191-8141(85)90023-9.

Smithies, R. H., and L. Bagas (1997), High pressure amphibolite-granulite facies metamorphism in the Paleoproterozoic Rudall Complex, central Western Australia, *Precambrian Res.*, *83*(4), 243–265, doi:10.1016/S0301-9268(96)00051-4.

Smithies, R. H., H. M. Howard, P. M. Evins, C. L. Kirkland, D. E. Kelsey, M. Hand, M. T. D. Wingate, A. S. Collins, and E. Belousova (2011), High-temperature granite magmatism, crust-mantle interaction and the Mesoproterozoic intracontinental evolution of the Musgrave Province, Central Australia, *J. Petrol.*, *52*(5), 931–958, doi:10.1093/petrology/egr010.

Smithson, S. B., J. Brewer, S. Kaufman, J. Oliver, and C. Hurich (1978), Nature of the Wind River thrust, Wyoming, from COCORP deep-reflection data and from gravity data, *Geology*, *6*, 648–652, doi:10.1130/0091-7613(1978)6<648:NOTWRT>2.0.CO;2.

Sprigg, R. C., B. Wilson, R. P. Coats, B. P. Webb, and E. S. O'Driscoll (1959) *4 Mile Geological Series Sheet. Alberga G 53–9 Zone 4*, 1st ed., Geol. Surv. of South Aust., Adelaide.

Stein, S., and A. E. Okal (2005), Speed and size of the Sumatra earthquake, *Nature*, *434*, 581–582, doi:10.1038/434581a.

Stewart, A. J. (1995), Western extension of the Woodroffe Thrust, Musgrave Block, central Australia, *AGSO J. Aust. Geol. Geophys.*, *16*(1/2), 147–153.

Stewart, A. J. (1997), *Record 1997/5: Geology of the Bates 1:100 000 Sheet Area (4646), Musgrave Block, Western Australia*, 1st ed., Aust. Geol. Surv. Organ., Canberra.

Sun, S., and J. Sheraton (1992), Zircon U/Pb chronology, tectono-thermal and crust-forming events in the Tomkinson Ranges, Musgrave Block, Central Australia, *AGSO Res. Newsl.*, *17*, 9–11.

Sun, S., J. W. Sheraton, A. Y. Glikson, and A. J. Stewart (1996), A major magmatic event during 1050–1080 Ma in central Australia, and an emplacement age for the Giles Complex, *AGSO Res. Newsl.*, *24*, 13–15.

Tikoff, B., P. Kelso, C. Manduca, M. J. Markley, and J. Gillaspy (2001), Lithospheric and crustal reactivation of an ancient plate boundary: The assembly and disassembly of the Salmon River suture zone, Idaho, USA, in *The Nature and Tectonic Significance of Fault Zone Weakening*, edited by R. E. Holdsworth et al., *Geol. Soc. London Spec. Publ.*, 186, 213–231.

Todd, C. S. (1998), Limits on the precision of geobarometry at low grossular and anorthite content, *Am. Mineral.*, *83*(11–12 Part 1), 1161–1167, doi:10.2138/am-1998-11-1203.

Trepmann, C. A., and B. Stöckhert (2002), Cataclastic deformation of garnet: A record of synseismic loading and postseismic creep, *J. Struct. Geol.*, *24*(11), 1845–1856, doi:10.1016/S0191-8141(02)00004-4.

Twiss, R. J., and E. M. Moores (2007), *Structural Geology*, 2nd ed., Freeman, New York.

van Lamoen, H. (1979), Coronas in olivine Gabbros and iron ores from Susimäki and Riuttamaa, Finland, *Contrib. Mineral. Petrol.*, *68*(3), 259–268, doi:10.1007/BF00371546.

Vigny, C., et al. (2005), Insight into the 2004 Sumatra-Andaman earthquake from GPS measurements in southeast Asia, *Nature*, *436*, 201–206, doi:10.1038/nature03937.

Voll, G. (1976), Recrystallization of quartz, biotite and feldspars from Erstfeld to the Leventina nappe, Swiss Alps, and its geological significance, *Schweiz. Mineral. Petrogr. Mitt.*, *56*(3), 641–647, doi:10.5169/seals-43709.

Wells, A. T., D. J. Forman, L. C. Ranford, and P. J. Cook (1970), *Bulletin 100: Geology of the Amadeus Basin, Central Australia*, Bur. of Miner. Resour., Geol. and Geophys., Canberra.

Wex, S., N. Mancktelow, F. Hawemann, A. Camacho, and G. Pennacchioni (2014), Pseudotachylyte formation vs. mylonitization - Repeated cycles of seismic fracture and aseismic creep in the middle crust (Woodroffe Thrust, Central Australia), *Geophys. Res. Abstr.*, *16*, 5071.

White, R. W., and G. L. Clarke (1997), The role of deformation in aiding recrystallization: An example from a high-pressure shear zone, Central Australia, *J. Petrol.*, *38*(10), 1307–1329, doi:10.1093/petrology/38.10.1307.

Whitney, D. L., and B. W. Evans (2010), Abbreviations for names of rock-forming minerals, *Am. Mineral.*, *95*(1), 185–187, doi:10.2138/am.2010.3371.

Wilson, A. F., and D. R. Hudson (1967), The discovery of beryllium-bearing sapphirine in the granulites of the Musgrave Ranges (central Australia), *Chem. Geol.*, *2*, 209–215, doi:10.1016/0009-2541(67)90022-8.

Winkler, H. G. F. (1979), *Petrogenesis of Metamorphic Rocks*, 5th ed., Springer, New York.

Worley, B., and R. Powell (2000), High-precision relative thermobarometry: Theory and a worked example, *J. Metamorph. Geol.*, *18*(1), 91–101, doi:10.1046/j.1525-1314.2000.00239.x.

Wu, C.-M., and B.-H. Cheng (2006), Valid garnet-biotite (GB) geothermometry and garnet-aluminum silicate-plagioclase-quartz (GASP) geobarometry in metapelitic rocks, *Lithos*, *89*(1–2), 1–23, doi:10.1016/j.lithos.2005.09.002.

Wu, C.-M., J. Zhang, and L.-D. Ren (2004), Empirical Garnet-Biotite-Plagioclase-Quartz (GBPQ) geobarometry in medium- to high-grade metapelites, *J. Petrol.*, *45*(9), 1907–1921, doi:10.1093/petrology/egh038.

Wyborn, L. A. I., R. W. Page, and A. J. Parker (1987), Geochemical and geochronological signatures in Australian Proterozoic igneous rocks, in *Geochemistry and Mineralization of Proterozoic Volcanic Suites*, edited by T. C. Pharaoh, R. D. Beckinsale, and D. Rickard, *Geol. Soc., London Spec. Publ.*, 33, 377–394.

Young, D. N., N. Duncan, A. Camacho, P. A. Ferenczi, and T. L. A. Madigan (2002) *1:250 000 Geological Map Series and Explanatory Notes. Ayers Rock SG 52–8*, 2nd ed., North. Territ. Geol. Surv., Darwin.

Zhao, J., and M. T. McCulloch (1993), Sm-Nd mineral isochron ages of Late Proterozoic dyke swarms in Australia: Evidence for two distinctive events of mafic magmatism and crustal extension, *Chem. Geol.*, *109*(1–4), 341–354, doi:10.1016/0009-2541(93)90079-X.

Zhao, J., M. T. McCulloch, and R. J. Korsch (1994), Characterisation of a plume-related ~ 800 Ma magmatic event and its implications for basin formation in central-southern Australia, *Earth Planet. Sci. Lett.*, *121*(3–4), 349–367, doi:10.1016/0012-821X(94)90077-9.